

Cite this: DOI: 00.0000/xxxxxxxxxx

# The diverse chemistry of protoplanetary disks as revealed by JWST

Ewine F. van Dishoeck,<sup>\*a,b</sup> S. Grant<sup>b</sup>, B. Tabone<sup>c</sup>, M. van Gelder<sup>a</sup>, L. Francis<sup>a</sup>, L. Tychoniec<sup>d</sup>, G. Bettoni<sup>b</sup>, A.M. Arabhavi<sup>e</sup>, D. Gasman<sup>f</sup>, P. Nazari<sup>a</sup>, M. Vlasblom<sup>a</sup>, P. Kavanagh<sup>g</sup>, V. Christiaens<sup>h</sup>, P. Klaassen<sup>i</sup>, H. Beuther<sup>j</sup>, Th. Henning<sup>j</sup>, and I. Kamp<sup>e</sup>

Received Date  
Accepted Date

DOI: 00.0000/xxxxxxxxxx

Early results from the JWST-MIRI guaranteed time programs on protostars (JOYS) and disks (MINDS) are presented. Thanks to the increased sensitivity, spectral and spatial resolution of the MIRI spectrometer, the chemical inventory of the planet-forming zones in disks can be investigated with unprecedented detail across stellar mass range and age. Here data are presented for five disks, four around low-mass stars and one around a very young high-mass star. The mid-infrared spectra show some similarities but also significant diversity: some sources are rich in CO<sub>2</sub>, others in H<sub>2</sub>O or C<sub>2</sub>H<sub>2</sub>. In one disk around a very low-mass star, booming C<sub>2</sub>H<sub>2</sub> emission provides evidence for a “soot” line at which carbon grains are eroded and sublimated, leading to a rich hydrocarbon chemistry in which even di-acetylene (C<sub>4</sub>H<sub>2</sub>) and benzene (C<sub>6</sub>H<sub>6</sub>) are detected<sup>1</sup>. Together the data point to an active inner disk gas-phase chemistry that is closely linked to the physical structure (temperature, snowlines, presence of cavities and dust traps) of the entire disk and which may result in varying CO<sub>2</sub>/H<sub>2</sub>O abundances and high C/O ratios >1 in some cases. Ultimately, this diversity in disk chemistry will also be reflected in the diversity of the chemical composition of exoplanets.

## 1 Introduction

Planets are built from gas and solids in the rotating disks around young stars. Their composition thus depends on the gas-grain chemistry that takes place in disks, which is known to change with position due to strong gradients in temperature, density and UV irradiation (e.g., refs.<sup>2–4</sup>). This chemistry may also change with evolutionary state: it is now well established that disks form early, already in the embedded state of star formation when the disk is still warmer<sup>5</sup> and surrounded by a larger scale envelope

that can feed the disk with fresh material. Planetary cores are likely formed at these early stages as well<sup>6</sup>. The study of the chemistry of planet formation must therefore encompass the entire sequence of star formation, from cold collapsing clouds to warm circumstellar disks.

The *James Webb Space Telescope* (JWST) offers new opportunities to study the chemistry of the warm inner regions of disks, typically within a few au\* radius from a solar-type star. This inner disk is the region in which most planets – both gas giants and terrestrial planets – are thought to form<sup>7,8</sup>. Compared with the *Spitzer* Space Telescope, which revealed that inner disks can have a very rich chemistry<sup>9–11</sup>, the JWST spectrometers have higher spectral resolving power ( $R = \lambda/\Delta\lambda \approx 2000 - 4000$  versus 60 – 600) and more than two orders of magnitude higher sensitivity, combined with an order of magnitude higher spatial resolution. JWST also complements the Atacama Large Millimeter/submillimeter Array (ALMA) which resolves millimeter-sized dust emission in disks down to a few au but which probes chemistry primarily beyond ~10 au (e.g., refs.<sup>12,13</sup>).

We present here some first results of the chemistry in the inner regions of disks based on JWST data from the Medium Resolution Spectrometer (MRS)<sup>14</sup> that is part of the Mid-InfraRed Instrument (MIRI)<sup>15,16</sup>. The data come from two guaranteed time

<sup>a</sup>Leiden Observatory, Leiden University, P.O. Box 9513, 2300 RA Leiden, the Netherlands. E-mail: ewine@strw.leidenuniv.nl

<sup>b</sup>Max-Planck Institut für Extraterrestrische Physik (MPE), Giessenbachstr. 1, 85748, Garching, Germany.

<sup>c</sup>Université Paris-Saclay, CNRS, Institut d’Astrophysique Spatiale, 91405, Orsay, France.

<sup>d</sup>European Southern Observatory, Karl-Schwarzschild-Strasse 2, 85748 Garching bei München, Germany.

<sup>e</sup>Kapteyn Astronomical Institute, Rijksuniversiteit Groningen, P.O. Box 800, 9700 AV Groningen, The Netherlands.

<sup>f</sup>Institute of Astronomy, KU Leuven, Celestijnenlaan 200D, 3001 Leuven, Belgium.

<sup>g</sup>Dublin Institute for Advanced Studies, Astronomy & Astrophysics Section, 31 Fitzwilliam Place, Dublin 2, Ireland.

<sup>h</sup>STAR Institute, Université de Liège, Allée du Six Août 19c, 4000 Liège, Belgium.

<sup>i</sup>UK Astronomy Technology Centre, Royal Observatory Edinburgh, Blackford Hill, Edinburgh EH9 3HJ, UK.

<sup>j</sup>Max-Planck-Institut für Astronomie (MPIA), Königstuhl 17, 69117 Heidelberg, Germany.

\* 1 astronomical unit (au) = distance Sun–Earth = 1.5 × 10<sup>13</sup> cm

programs: the “JWST Observations of Young protoStars” (JOYS) program (PIs: E.F. van Dishoeck and H. Beuther, program id: 1290), which targets two dozen young disks and their envelopes and outflows in the embedded stage of low- and high-mass star formation<sup>17</sup>, and the MIRI Infrared Disk Survey (MINDS) (PIs: Th. Henning and I. Kamp, program id: 1282), which observes about 50 disks around pre-main sequence stars across a range of stellar masses and ages<sup>18,19</sup>. Here high mass refers to stars of O and B spectral type (typical masses  $8 M_{\odot}$  and higher) or protostars with total luminosities greater than a few  $\times 10^3 L_{\odot}$ . At the time of submission of this paper (January 2023), only one JOYS source has been observed—the high-mass protostar IRAS 23385+6052<sup>20</sup>—, and data for a dozen MINDS sources have been taken, although none of them are disks that were found to be particularly line rich with *Spitzer* like AA Tau<sup>9</sup>. Here we present results on small molecules, most notably CO<sub>2</sub>, H<sub>2</sub>O and hydrocarbons, as observed toward IRAS 23385+6052, and from disks around the T Tauri stars GW Lup, V1094 Sco, Sz 98 and the very low-mass star 2MASS-J16053215-1933159. Even within this limited sample observed so far, the data show the diversity of spectra and disk chemistry, not just among T Tauri disks but also across a range of stellar masses.

## 2 Observations and methods

### 2.1 JWST data reduction

The MIRI-MRS consists of four Integral Field Units (IFUs) (also called “channels”) covering different wavelength ranges within the 4.9–28.1  $\mu\text{m}$  (355–2040  $\text{cm}^{-1}$ ) range. The Field-of-View (FOV) varies between the four channels from  $3.2'' \times 3.7''$  covered with 21 IFU slices of  $0.18''$  at the shortest wavelengths, to  $6.6'' \times 7.7''$  observed with 12 slices of  $0.66''$  width at the longest wavelengths. Thus, the MIRI-MRS provides spectral images on arcsec scales but in this paper only point-source spectra centered on the disks are presented. Full wavelength coverage was obtained in three grating moves that are observed simultaneously for all four channels. The FASTR1 readout pattern was used with a 2-point dither pattern in JOYS and a 4-point dither pattern in MINDS.

IRAS 23385+6052 (luminosity  $L=3 \times 10^3 L_{\odot}$ , distance  $d=4.9 \text{ kpc}$ <sup>†</sup><sup>21</sup>, age  $\text{few} \times 10^4 \text{ yr}$ , hereafter IRAS 23385) was observed as part of JOYS on August 22, 2022. This source actually consists of a small cluster of protostars, as revealed from previous millimeter<sup>20,22</sup> and near-infrared images<sup>23</sup>, with the most massive protostar estimated to be  $9 M_{\odot}$  from Keplerian rotation measurements of the surrounding gas<sup>20</sup>. Note that this source is too far north to be observable by ALMA. The total exposure time in each MRS grating setting was 200 sec.

The spectra toward GW Lup ( $M_{*}=0.46 M_{\odot}$ ,  $L=0.33 L_{\odot}$ <sup>24</sup>,  $d=155 \text{ pc}$ ), V1094 Sco ( $M_{*} \approx 0.9 M_{\odot}$ ,  $L=1.7 L_{\odot}$ <sup>24</sup>,  $d=153 \text{ pc}$ ), Sz 98 ( $M_{*} \approx 0.74 M_{\odot}$ ,  $L=1.5 L_{\odot}$ <sup>24</sup>,  $d=155 \text{ pc}$ ), and 2MASS-J16053215-1933159 ( $M_{*}=0.14 M_{\odot}$ ,  $L=0.04 L_{\odot}$ <sup>25</sup>,  $d=152 \text{ pc}$ , hereafter J160532) were taken as part of the MINDS program on 2022 August 8 and August 1 for a total of  $\sim 2 \text{ hr}$  each includ-

ing overheads (typically 800–1200 sec per grating setting). The distances to these sources come from the Gaia DR3 catalogue<sup>26</sup>, whereas their ages are all typically a few Myr<sup>24,27</sup>.

The MIRI-MRS observations of all JOYS and MINDS sources were processed through the three reduction stages<sup>28</sup> using Pipeline version 1.8.4 of the JWST Science Calibration Pipeline<sup>43</sup> and the CRDS context `jwst_1017.pmap`. Prior to processing J160532, the background was removed using pair-wise dither subtraction. The default class `Spec2` was applied, skipping the residual fringe correction. Instead, for GW Lup, V1094 Sco, and Sz 98, the alternative reference files as discussed in Gasman et al.<sup>29</sup> were applied, which correct the fringes sufficiently in `Spec2`. The data were then processed by the `Spec3` class, which combines the calibrated data from the different dither observations into a final level3 spectral cube. The `outlier_detection` and `master_background` methods were skipped, since for both MINDS and JOYS this was done manually. Finally, a manual extraction of the spectra for each sub-band was performed, including aperture correction, with an aperture size of  $2.5\lambda/D$  for the low-mass sources. The backgrounds of GW Lup, V1094 Sco, and Sz 98 were estimated using an annulus around the source, with an appropriate aperture correction accounting for the PSF signal present in the annulus.

The high-mass protostar IRAS 23385 turns out to be a binary source with a separation of  $\sim 0.67''$  ( $\sim 3280 \text{ au}$ ) at mid-infrared wavelengths. This means that the binary is resolved in Channel 1 and part of Channel 2, but that the system is unresolved at longer wavelengths. The spectrum presented here was extracted using a circular aperture of  $2.4''$  diameter independent of wavelength that includes both sources. Background subtraction was done using the emission measured at off-source positions within the IFUs. This turned out to be more reliable than subtraction using the complementary dark field that was observed but that still contained strong extended emission. A residual fringe correction was applied at the spectrum level. More details for IRAS 23385 can be found in Beuther et al.<sup>30</sup>, and for the MINDS sources in Grant et al.<sup>31</sup> and Tabone et al.<sup>1</sup>.

### 2.2 Methods

The mid-infrared wavelength range observed by MIRI-MRS covers the vibration-rotation bands of many molecules, from simple molecules like CO and CO<sub>2</sub> to more complex aliphatic and aromatic hydrocarbon molecules. For H<sub>2</sub>O and OH, also pure rotational transitions between high-lying levels within the ground vibrational state are observable beyond  $10 \mu\text{m}$ .

The continuum-subtracted spectra were fitted with slab models of the molecular emission that take optical depth effects and line overlap into account, following the methods used for analyzing *Spitzer* spectra<sup>10,32</sup>. The populations of the molecular levels are assumed to be characterized by a single excitation temperature,  $T_{\text{ex}}$ , which is taken to be equal to the gas temperature  $T$  assuming Local Thermodynamic Equilibrium (LTE). Note that radiative pumping of the lines may also be significant in the inner disk<sup>33</sup>, in which case  $T_{\text{ex}}$  approaches the temperature of the radiation field,  $T_{\text{rad}}$ .

<sup>†</sup> 1 parsec = 206265 au = 3.26 lightyear =  $3.086 \times 10^{18} \text{ cm}$

The line profile function is taken to be Gaussian with a full width at half maximum of  $\Delta V = 4.7 \text{ km s}^{-1}$  ( $\sigma = 2 \text{ km s}^{-1}$ ), as in previous *Spitzer* studies. At high optical depth, the line shape becomes a flat-topped pseudo-Gaussian due to saturation at the line core. These models have only three free parameters: the line of sight column density  $N$ , the gas temperature  $T$ , and the emitting area given by  $\pi R^2$ . It is stressed that  $R$  does not necessarily correspond to a disk radius, but that the emission could come from a ring or any other region with an area equivalent to  $\pi R^2$ .

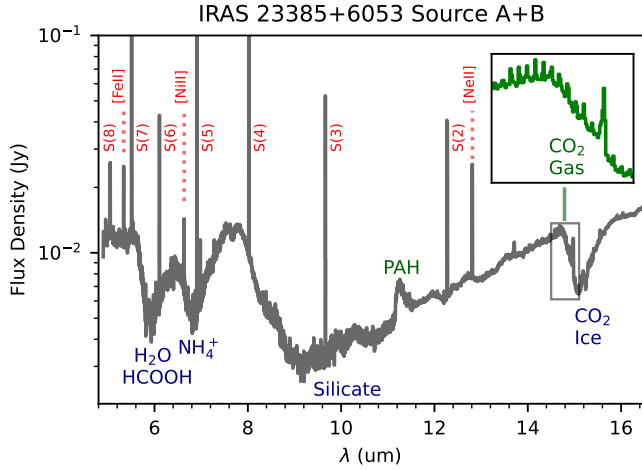


Fig. 1 Part of the MIRI-MRS spectrum toward the high-mass protostar IRAS 23385+6053 integrated over both sources. Blue labels refer to ice and solid-state absorption features, red to spatially extended narrow emission lines, and green to molecular emission with  $\text{CO}_2$  centered on the sources and PAH emission extended.

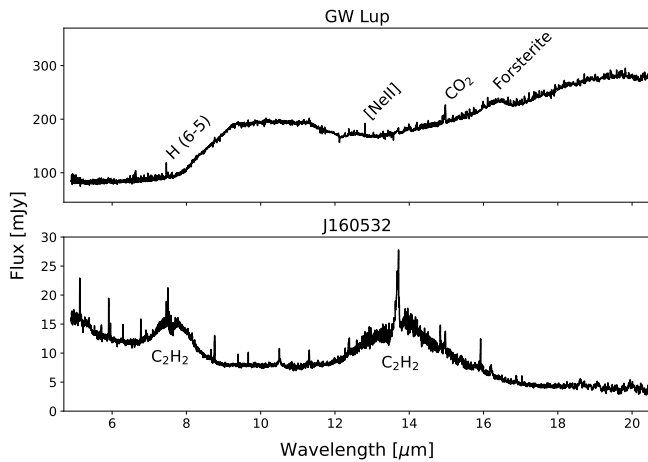


Fig. 2 MIRI-MRS 5–20  $\mu\text{m}$  spectrum of the disk around the T Tauri star GW Lup<sup>31</sup> compared with that of the very low-mass star J160532 presented by ref.<sup>1</sup>. The GW Lup spectrum shows amorphous silicate emission at 10 and 18  $\mu\text{m}$  with superposed atomic and molecular lines as well as some crystalline forsterite emission. The broadband J160532 spectrum shows no silicate emission but two prominent bumps that can be ascribed to very abundant  $\text{C}_2\text{H}_2$  emission<sup>1</sup>.

The molecular data, i.e., energy levels, statistical weights, Einstein A coefficients and partition functions, were taken from the

HITRAN 2020 database<sup>34</sup> and converted into LAMDA format<sup>35</sup>. For  $\text{C}_6\text{H}_6$ , molecular parameters based on the GEISA database were used<sup>36</sup>. Integrated line fluxes are computed, varying the emitting area and taking the known distances to the sources into account. The model spectrum is then convolved to the instrumental spectral resolving power<sup>37</sup> and the convolved model spectrum is resampled to have the same wavelength grid as the observed spectrum. Model grids were run for each molecule with  $T$  from 100 to 1500 K,  $N$  from  $10^{14}$  to  $10^{22} \text{ cm}^{-2}$ , and emitting radius from 0.01 to 10 au for the low-mass sources. For the high-mass source, these ranges are 50–550 K,  $10^{14}$ – $10^{20} \text{ cm}^{-2}$  and 0.01–10000 au. The best-fit  $N$  and  $T$  are determined using a  $\chi^2$  fit between the continuum subtracted data and the convolved and resampled model spectrum, using the best-fit emitting area for each  $N$  and  $T$ . The procedure is iterative, starting with fitting those molecules that have the most lines in a certain wavelength range that are overlapping with those of others, and ending with the weaker features. More details can be found in refs.<sup>1,31</sup>.

### 3 Results

#### 3.1 Broad-band spectra

Figure 1 presents part of the observed MIRI-MRS spectrum toward the high-mass binary protostar IRAS 23385<sup>30</sup>. Note that this source is more than a factor of 1000 weaker than the high-mass protostars studied with ISO<sup>38</sup>, only  $\sim 10 \text{ mJy}$ , demonstrating the JWST sensitivity. As is typical for a deeply embedded young stellar object, the spectrum is rising with wavelength due to the thermal emission from dust surrounding the binary protostar which has a temperature gradient from warm to cold<sup>39</sup>. Superposed on this continuum are deep and broad absorption bands due to silicates and a variety of ices arising in the cold outer envelope<sup>40,41</sup>. A number of strong, narrow emission lines due to various atoms and  $\text{H}_2$  are seen as well, associated with shocks due to the outflows from the protostars. Finally, PAH emission from a background cloud is seen at 11.3 and 8.6  $\mu\text{m}$ <sup>42</sup>; the shorter wavelength PAH features are blocked by the high extinction and deep ice features in the envelope. Both the absorptions and spatially extended gas-phase lines will be described elsewhere<sup>30,43</sup>.

Figure 2 compares the MIRI-MRS spectra of two low-mass sources, GW Lup and J160532. The GW Lup spectrum is typical of that of a disk around a young star whose protostellar envelope has already been dissipated: its spectral energy distribution drops at long wavelengths but it shows strong, broad emission bands due to amorphous and crystalline silicates<sup>46–48</sup> in the MIRI range.

In contrast to most disk sources including V1094 Sco and Sz 98, the J160532 spectrum is unusual: it shows no silicate emission feature but has two broad bumps centered at 7.7 and 13.7  $\mu\text{m}$  as was already noted in low-resolution *Spitzer* data<sup>49,50</sup>. Tabone et al.<sup>1</sup> show that these bumps are due to the  $\nu_4 + \nu_5$  and  $\nu_5$  bands of  $\text{C}_2\text{H}_2$  respectively which is present at very high column densities ( $\sim 10^{21} \text{ cm}^{-2}$ ) and emitting at a temperature around 500 K within a small region of radius 0.033 au. In this optically thick component, the  $Q$ -branch is suppressed. The clearly visible  $Q$ -branch as well as other individual  $R$ - and  $P$ -lines (see below) require an additional optically thin  $\text{C}_2\text{H}_2$  component with a  $10^4$

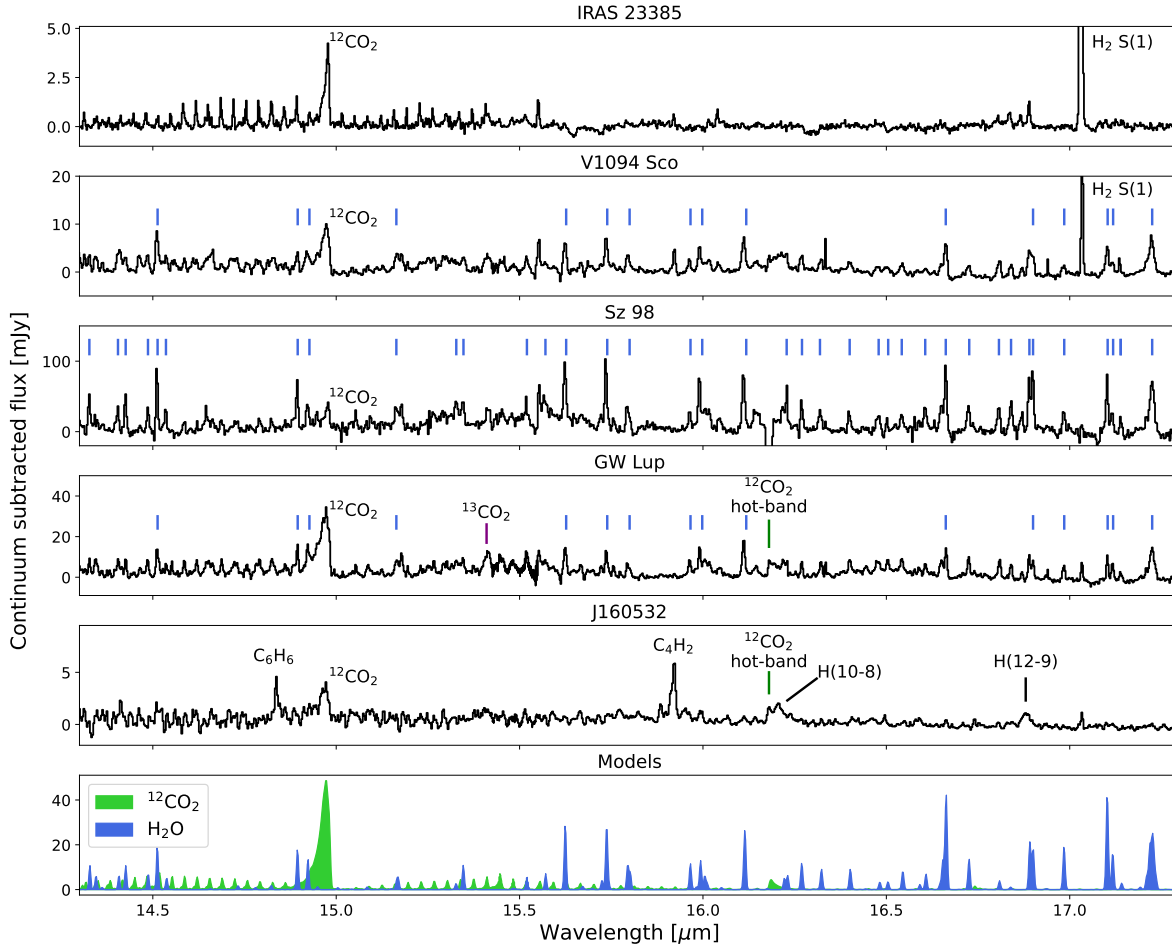


Fig. 3 Continuum-subtracted MIRI-MRS 14.3–17.3  $\mu\text{m}$  spectra of the young high-mass protostar IRAS 23385<sup>44</sup>, and of the disks around the T Tauri stars V1094 Sco, Sz 98<sup>45</sup> and GW Lup<sup>31</sup>, and the very low-mass star J160532<sup>1</sup>. The blue tickmarks in the V1094 Sco, Sz 98 and GW Lup panels indicate the locations of water lines. Note also the detected  $^{13}\text{CO}_2$  and hot bands of  $^{12}\text{CO}_2$  toward GW Lup<sup>31</sup>. The bottom panel shows simulated LTE slab model spectra of  $\text{CO}_2$  and  $\text{H}_2\text{O}$  at 600 K (arbitrary relative scaling).

times lower column density.

None of these disk spectra shows emission from polycyclic aromatic hydrocarbons (PAHs). However, this lack of PAH features does not imply absence of these molecules: as shown by Geers et al.<sup>51</sup>, the UV radiation from stars with  $T_{\text{eff}} < 4200$  K (spectral type later than K6, assuming no significant excess UV radiation due to accretion) is too weak to produce detectable PAH bands.

### 3.2 Identified molecules

Of interest to this paper are the series of weak narrow lines with a line/continuum ratio of less than 10 % on top of the continuum (see GW Lup spectrum in Figure 2). Figure 3 presents the continuum subtracted spectra in the 14.3–17.3  $\mu\text{m}$  range for the five sources discussed here, with various emission features labelled. Fig. 4 presents the spectrum of J160532 at 13.3–16.1  $\mu\text{m}$  including the prominent  $\text{C}_2\text{H}_2$   $Q$ -branch at 13.7  $\mu\text{m}$  with weak HCN at 14.0  $\mu\text{m}$ . The shorter wavelength parts of the spectra of the other sources showing  $\text{C}_2\text{H}_2$  and HCN are included in the paper by Kamp et al. (this volume).

The most prominent band in Figure 3 is the  $Q$ -branch of  $\text{CO}_2$  at 15  $\mu\text{m}$ . Its  $R$ - and  $P$ -branch lines are weaker but still visible, most notably in IRAS 23385. The  $Q$ -branches of the  $\text{CO}_2$  hot bands and of the 13-C isotopolog of  $\text{CO}_2$  are also detected in some sources, most notably GW Lup<sup>31</sup>. An irregular set of lines due to  $\text{H}_2\text{O}$  shows up most strongly in the Sz 98 disk, but these lines are also present in the GW Lup and V1094 Sco disks. In contrast, in the J160532 disk only a few weak  $\text{H}_2\text{O}$  lines are tentatively seen<sup>1</sup>, and none in IRAS 23385 in this wavelength range. The  $\text{H}_2$  S(1) line at 17.0  $\mu\text{m}$  and H I recombination lines are also seen in a few sources, as are some OH lines. Excitingly, bands of  $\text{C}_6\text{H}_6$  and  $\text{C}_4\text{H}_2$  are clearly detected in the J160532 disk (Figure 4), and  $\text{CH}_4$  emission is possibly found as well<sup>1</sup>. Many of these lines are seen with JWST for the first time in disks.

Note that the bulk of the lines in this wavelength range can be fit with these molecules. There could be additional lower abundance molecules present, or isotopologs of identified molecules, whose weaker lines are blended with the stronger lines and that have not yet been identified at this stage of data processing. Also,

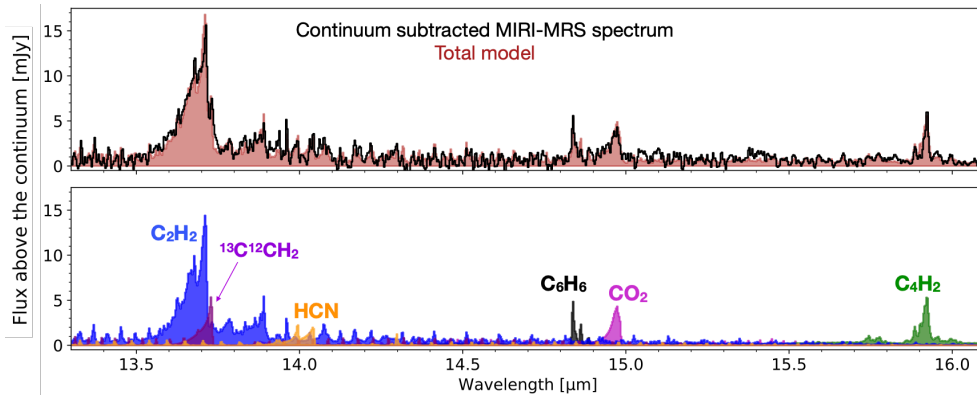


Fig. 4 Continuum-subtracted MIRI-MRS 13.3–16.1  $\mu\text{m}$  spectrum of the very low-mass star J160532, showing prominent features of  $\text{C}_2\text{H}_2$ ,  $\text{C}_4\text{H}_2$  and  $\text{C}_6\text{H}_6$ . The 13-C isotopolog of  $\text{C}_2\text{H}_2$  is also detected, as are HCN and  $\text{CO}_2$  (see ref.<sup>1</sup> for details). The big bump at 13.7  $\mu\text{m}$  (see Figure 2) due to very high column density  $\text{C}_2\text{H}_2$  component has been subtracted.

line lists of various potentially interesting molecules are currently unavailable or incomplete at high temperatures, especially for hydrocarbons (see also paper by Kamp et al. in this volume).

### 3.3 Inferred column densities and temperatures

Table 1 summarizes the inferred best-fitting column densities, temperatures and emitting areas of various molecules for two of the sources. An example of a typical  $\chi^2$  plot can be found in Figure 5. As found in previous studies based on *Spitzer* data<sup>10,32</sup>, there is a wide range of fit parameters that reproduce the spectra well. Most notably, in the low column density regime (typically  $< 10^{17} \text{ cm}^{-2}$  depending on molecule) where lines are optically thin, there is a complete degeneracy between column density and emitting radius. On the other hand, the latter can be determined from optically thick lines whose strength scales directly with emitting area. The temperature is often well constrained from the shape and position of the  $Q$ -branch feature, where lines with  $\Delta J=0$  pile up: the warmer the gas, the broader the feature. MIRI can resolve this  $Q$ -branch much better than before. An excellent example of the latter is provided by the  $\text{CO}_2$   $Q$ -branch toward IRAS 23385, which is only consistent with a low temperature of  $150 \pm 50 \text{ K}$ . The availability of both optically thick and thin lines with JWST as well as their 13-C isotopologs helps to resolve several of these degeneracies.

A few column density ratios are summarized in Table 2 to give an impression of the range of values, which will be discussed further below. For V1094 Sco, these column density ratios are obtained from a preliminary analysis assuming the same emitting radius of 0.13 au for all species. For more details, see refs.<sup>1,31,44</sup>.

## 4 Discussion

### 4.1 Diversity in spectra

Figures 1–4 illustrate the diversity in mid-infrared spectra of embedded protostars and young stars with disks, not just between these two classes of sources but even between disk-dominated sources themselves. High quality mid-infrared spectra are now possible for much fainter sources than before, down to mJy continuum level, thanks to JWST. Focusing just on the molecular

emission, one of the striking features of Figure 3 is the difference in the strength of  $\text{H}_2\text{O}$  emission in the 14.3–17.3  $\mu\text{m}$  region, with  $\text{H}_2\text{O}$  lines virtually absent in the spectra of the high mass binary IRAS 23385 and the very low-mass source J160532, but clearly present in those of GW Lup and V1094 Sco and dominant in Sz 98. Another obvious difference is the strength of the  $\text{C}_2\text{H}_2$  band with respect to other features, with  $\text{C}_2\text{H}_2$  and hydrocarbons dominating the spectrum of the very low-mass star J160532 but being much weaker toward other sources (see paper by Kamp et al., this volume).  $\text{CO}_2$  is detected in all sources, most strongly relative to other features in the GW Lup disk.

How about nitrogen? One molecule that has not yet been detected in disks with MIRI is  $\text{NH}_3$  whose  $\nu_6$  mode at 8.8  $\mu\text{m}$  can now be observed at much higher spectral resolution with the MRS than was possible with *Spitzer*. The HCN  $Q$ -branch at 14.0  $\mu\text{m}$  is seen in most sources but is now recognized to be heavily blended with both  $\text{C}_2\text{H}_2$ ,  $\text{CO}_2$  and/or  $\text{H}_2\text{O}$  lines (Figure 4) resulting in an HCN contribution that is smaller than thought based on *Spitzer* data<sup>10,52</sup>. This means that an even lower fraction of nitrogen has been identified than before, suggestion that the bulk of the nitrogen in the inner disk may well be in the unobservable  $\text{N}_2$  form<sup>53</sup>.

Where does the molecular emission originate? For the low-mass sources, the lines clearly come from the inner region of their disks, typically within 1 au, as is also evidenced by their small emitting areas (Table 1). Although the emission could in principle also come from a narrow ring further out in the disks, the high inferred temperatures also point to a location in the inner disk.

For high-mass protostars, the emitting area of only 35 au radius is also relatively small. Interestingly, for high-mass protostars these molecular bands are often seen in absorption rather than emission in spectra taken with the *Infrared Space Observatory*<sup>54–56</sup>. Those lines were thought to originate in the inner warm envelope where ices have sublimated (“hot core”) or in shocked gas along the line of sight seen in absorption toward the strong mid-infrared continuum due to hot dust close to the protostars. However, more recent high spectral resolution ground-based and SOFIA-EXES data suggest an origin in the inner part of a disk around the massive young star<sup>57,58</sup>. Weak water absorption at 6  $\mu\text{m}$  is seen toward IRAS 23385 but only towards source

Table 1 Best fit molecular model parameters

Molecule	IRAS 23385			GW Lup		
	$N$ ( $\text{cm}^{-2}$ )	$T$ (K)	$R$ (au)	$N$ ( $\text{cm}^{-2}$ )	$T$ (K)	$R$ (au)
CO <sub>2</sub>	1E17	150	35	1E18	475	0.09
H <sub>2</sub> O	<1E18	[150]	[35]	2E18	625	0.16
C <sub>2</sub> H <sub>2</sub>	7E16	210	8	4E17	550	0.05

Note: brackets indicate parameters that were fixed in the fit.

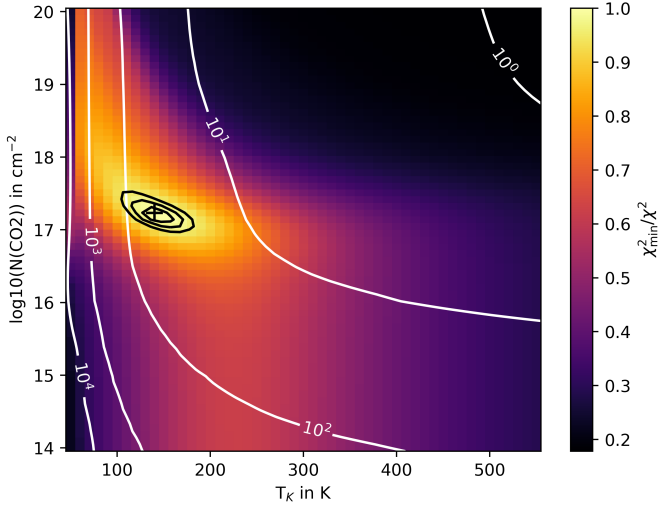


Fig. 5 Example of a  $\chi^2$  map to constrain temperature and column density, here for the case of CO<sub>2</sub> in IRAS 23385. The white lines indicate the best fitting emitting areas for those  $N$ ,  $T$  combinations. The black lines indicate the  $1\sigma$ ,  $2\sigma$  and  $3\sigma$  contours.

B of the binary<sup>44</sup>. Emission lines of CO<sub>2</sub>, C<sub>2</sub>H<sub>2</sub> and HCN at 13–15  $\mu\text{m}$  have previously been seen only toward the Orion peak 1 and 2 shock positions away from the strong continuum<sup>59</sup> and in the Cepheus A high-mass region<sup>60,61</sup>. Interestingly, in both cases moderate excitation temperatures of  $\sim 200$  K were found, lower than those seen for absorption bands, and similar to those derived here. For IRAS 23385, the molecular emission is clearly centered on the two protostars and is not detected in off-source shock positions<sup>44</sup>. Also, the lack of strong H<sub>2</sub>O emission, universally observed to be associated with shocks<sup>62</sup>, argues against an outflow origin. Although we cannot exclude a shock origin at this stage, we assume here that the emission originates in the disk(s) around (at least one of) the protostars in the IRAS 23385 system.

Table 2 Column density ratios of various molecules

Ratios	IRAS23385	V1094Sco	GW Lup	J160532
CO <sub>2</sub> /H <sub>2</sub> O	>0.1	0.004	0.45	>0.1
CO <sub>2</sub> /C <sub>2</sub> H <sub>2</sub>	1.7	0.1	2.2	0.0001

Note: column density ratios do not reflect local abundance ratios. For J160532, the optically thick C<sub>2</sub>H<sub>2</sub> component is used to compute the ratio.

## 4.2 Diversity in chemistry

Table 2 summarizes the column density ratios of the main molecules considered here in four of the sources. Uncertainties are up to an order of magnitude, based on the  $\chi^2$  plots. It should

be stressed that these ratios should not be equated with abundance ratios since the emission of different molecules (or even of different bands of the same molecule) may originate from different regions or layers of the disk<sup>33,63</sup>. Moreover, the emission seen at mid-infrared wavelengths only probes the upper layers of the disk above the  $\tau_{\text{mid-IR}} = 1$  contour where the dust continuum becomes optically thick.

In spite of these considerations, the similarities and differences in mid-infrared spectra can give some insight into the chemical processes at play in planet-forming zones of disks, especially since the differences in column density ratios are much larger than those of flux ratios of optically thick lines. As concluded from the appearance of the spectra, the J160532 inner disk is particularly rich in C<sub>2</sub>H<sub>2</sub>, whereas the V1094 Sco has the lowest CO<sub>2</sub>/H<sub>2</sub>O ratios, with Sz 98 likely even lower<sup>45</sup>. Apart from the larger size of the emitting region, the high-mass source IRAS 23385 does not stand out in terms of its abundance ratios compared with the orders of magnitude lower luminosity T Tauri sources.

GW Lup is part of a handful of sources that were found by *Spitzer* to have strong CO<sub>2</sub> emission but no emission from other molecules, the so-called “CO<sub>2</sub>-only” sources<sup>10</sup>. Thanks to the detection of <sup>12</sup>CO<sub>2</sub> hot bands, its  $P$ - and  $R$ -branch lines and the <sup>13</sup>CO<sub>2</sub>  $Q$ -branch, the inferred CO<sub>2</sub> column density is two orders of magnitude higher (and emitting area smaller) than found in analyses of the *Spitzer* data, illustrating the importance of the additional weaker optically thin features now observed with MIRI-MRS<sup>31</sup>. H<sub>2</sub>O and other molecules are now weakly detected as well with JWST, but its CO<sub>2</sub>/H<sub>2</sub>O column density ratio remains clearly higher than that of other low-mass sources.

## 4.3 Chemical processes

### 4.3.1 Disk models.

The chemistry in disks is known to vary both radially and vertically owing to large gradients in temperature, density and UV irradiation. A detailed 2D (or axisymmetric 3D) model of the physical structure of a disk therefore needs to be constructed before the chemistry can be addressed. Such thermochemical models have been developed for disks around low-mass stars by various groups<sup>64–67</sup>, with some of them focused specifically on inner disk chemistry where high-temperature gas-phase chemistry dominates<sup>63,68–72</sup>. Snowlines, i.e., the location in the disk where 50% of the molecule is in the gas and 50% in the ice, play an important role in setting the overall gas-phase chemical composition. Of particular interest is the C/O ratio in volatiles (i.e., gas + ices), since ices naturally lock up more oxygen than carbon<sup>73</sup>. For CO, whose pure ice binding energy is  $E/k \approx 855$  K<sup>74</sup>,

its snowline lies around 20 K which is typically at tens of au in a disk around a low-mass star<sup>75</sup>. For H<sub>2</sub>O, whose binding energy is much higher at  $E/k \approx 5600$  K<sup>76</sup>, its snowline is at  $\sim 160$  K at the high densities in disk midplanes, located at less than a few au<sup>77</sup>. The snowlines of other molecules like CO<sub>2</sub> generally lie in between those of CO and H<sub>2</sub>O<sup>78</sup>, with the exception of those of large organic molecules. In particular, the “soot” line due to sublimation and erosion of refractory hydrocarbon material is thought to lie around 500 K in disks<sup>79</sup>.

If  $R$  listed in Table 1 is taken to be a disk radius, the emission observed here for low-mass stars originates from well inside the H<sub>2</sub>O snowline. At these radii and temperatures, much of the oxygen that was locked up in ices should have returned to the gas phase<sup>73</sup>. The overall (gas + ices + refractory dust) C/O ratio in disks is expected to be similar to the stellar value, which in turn should be close to the solar value of C/O=0.59 within the solar neighborhood<sup>80</sup>. For gas-phase chemistry outside the refractory dust sublimation radius, only the volatile (gas + ice) C/O ratio is relevant, which is generally taken to be somewhat lower than 0.6 in disk models. Its precise value does not matter much for the chemistry and mid-infrared line emission<sup>63,72</sup> as long as C/O < 1.

It is important to note that any disk model reproducing mid-infrared lines needs to have a gas/dust ratio in the upper layers that is significantly higher than the standard interstellar medium value of 100, typically<sup>33,63,81</sup> of order  $10^3 - 10^4$ . Such high gas/dust ratios are naturally explained by grain growth and settling to the midplane<sup>82</sup>.

The physical and chemical structure of disks around high-mass O and B stars has not been modeled in as much detail as that of disks around A- and later-type stars<sup>71</sup>. An additional complication for such high-mass stars is that they are much younger and do not have an optically visible pre-main sequence stage. Although disks are commonly found to form in simulations of high-mass star formation<sup>83,84</sup>, they are still embedded in their natal envelopes. Moreover, accretion rates are still high, so heating of their inner disk midplane is dominated by viscous processes rather than passive irradiation<sup>85</sup>. Figure 7 compares the 2D dust temperature structure for one quadrant of a disk around a low-mass star with that of a high-mass star<sup>86,87</sup>, obtained using the RADMC-3D code<sup>88</sup>. The gas temperature is closely coupled to that of the dust except in the upper surface layers. For high-mass disks, the midplane is actually warmer than the surface layers within the inner  $\sim 100$  au<sup>87</sup> (depending on the accretion rate) giving rise to infrared absorption lines<sup>58</sup>. At larger radii, the disk switches to the usual structure of a vertically decreasing temperature structure from surface to midplane leading to mid-infrared emission lines. IRAS 23385 has a somewhat lower luminosity and accretion rate than assumed in the model in Figure 7, suggesting that the switch moves well inside 100 au.

#### 4.3.2 CO<sub>2</sub> versus H<sub>2</sub>O: cavities and dust traps.

Armed with the above background information on disk models, we now address the chemistry of the main species considered in this paper.

**4.3.2.1 Chemical processes relating CO<sub>2</sub> and H<sub>2</sub>O.** The temperature structure of the inner disk plays a crucial role in set-

ting the balance between the CO<sub>2</sub> and H<sub>2</sub>O abundances<sup>71,89</sup>. Both molecules are formed through gas-phase reactions with the OH radical<sup>71,90</sup>. At temperatures of 100–250 K, the OH + CO  $\rightarrow$  CO<sub>2</sub> + H reaction produces CO<sub>2</sub> with typical abundances of  $10^{-7} - 10^{-6}$  with respect to total H. At higher temperatures, the reaction OH + H<sub>2</sub>  $\rightarrow$  H<sub>2</sub>O + H, which has an energy barrier of 1740 K<sup>91</sup>, takes over and produces H<sub>2</sub>O in favor of CO<sub>2</sub>. Once H<sub>2</sub>O becomes abundant, its column density becomes high enough ( $\sim 10^{18}$  cm<sup>-2</sup>) to become self-shielding<sup>92</sup> pushing the balance even further toward H<sub>2</sub>O. Note that OH itself also needs moderately warm temperatures to form since the O + H<sub>2</sub>  $\rightarrow$  OH + H reaction is endothermic by 900 K and has an energy barrier as well<sup>91</sup>. Both the formation of OH and H<sub>2</sub>O are boosted by the presence of vibrationally excited H<sub>2</sub> where the vibrational energy can be used to overcome the energy barriers.

H<sub>2</sub>O and CO<sub>2</sub> are both abundant components of ices in cold interstellar clouds and protostellar envelopes<sup>41</sup>. A fraction of these ices are likely preserved in the transition from envelope to disk, especially for the stronger bound molecules like H<sub>2</sub>O<sup>93</sup>, as also illustrated by the similarity between interstellar and cometary ice abundances<sup>94,95</sup>. Inside their respective snowlines, the ice species sublimate and thus add to the gas-phase chemistry budget. Minor species intimately mixed with H<sub>2</sub>O ice sublimate together with water at its snowline<sup>96</sup>.

Bosman et al.<sup>89,98</sup> find that H<sub>2</sub>O mid-infrared emission dominates over CO<sub>2</sub> emission in the 13–17  $\mu$ m range for low-mass disks, if H<sub>2</sub>O self-shielding and efficient gas heating mechanisms are included. In particular, so-called (photo)chemical heating, in which the excess energy released by photodissociation and subsequent chemical reactions of the dissociation products is used to heat the gas<sup>99</sup>, can raise the temperatures in the upper layers significantly<sup>100</sup>.

**4.3.2.2 Role of small cavities.** Given the model predictions that H<sub>2</sub>O emission should dominate mid-infrared spectra, which processes could then make CO<sub>2</sub> more prominent than H<sub>2</sub>O in some disks but not others? One parameter that affects mid-infrared line fluxes is the amount of small grains in the upper layers. However, both CO<sub>2</sub> and H<sub>2</sub>O fluxes are decreased by comparable amounts if the gas/dust ratio is decreased<sup>101</sup>. Another option would be to change the C/O ratio, but again both CO<sub>2</sub> and H<sub>2</sub>O emission lines appear to be affected similarly<sup>63,72</sup>. Walsh et al.<sup>71</sup> show that for very low-mass stars H<sub>2</sub>O formation is indeed suppressed in the disk’s surface layers due to their lower temperatures, consistent the lowest-luminosity sources in our sample, GW Lup and J160532, showing the weakest H<sub>2</sub>O lines. However, some higher luminosity sources, including IRAS 23385, also show weak water emission.

An alternative explanation would be to introduce a deep dust + gas cavity in the inner disk, caused for example by a companion. Its radius needs to be in between that of the H<sub>2</sub>O and CO<sub>2</sub> snowlines in order to remove most of the H<sub>2</sub>O but not the CO<sub>2</sub> emission<sup>31,72,102</sup>. Figure 6 presents an example of the 2D abundance structure of H<sub>2</sub>O and CO<sub>2</sub> in a model<sup>97</sup> obtained using the DALI thermochemical code<sup>66</sup> for a disk with the same parameters as in Bosman et al.<sup>89</sup>. Two cases are presented: a full disk

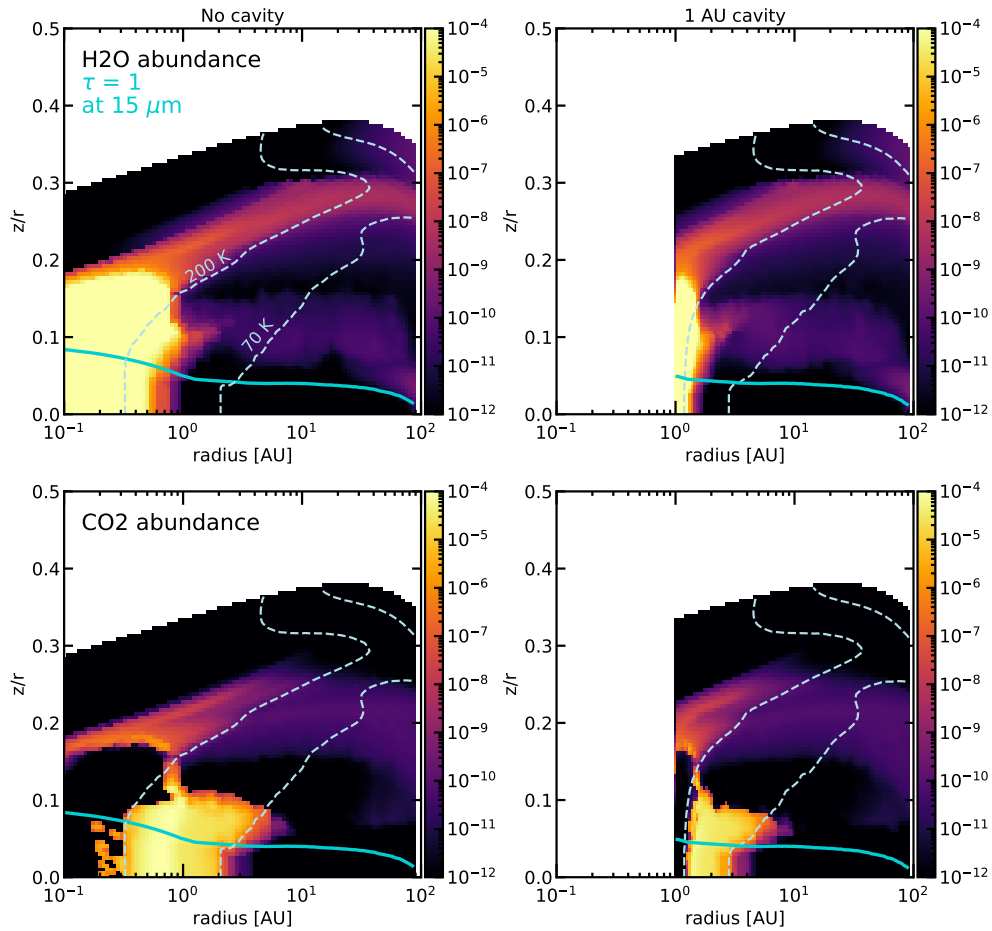


Fig. 6 Two dimensional map of the  $\text{H}_2\text{O}$  and  $\text{CO}_2$  abundances of one quadrant of a disk around a low-mass star without a cavity (left) and with a 1 au cavity (right)<sup>97</sup>. The dashed lines indicate the 70 and 200 K temperature contours; the blue line the  $\tau_{\text{mid-IR}} = 1$  line at  $15 \mu\text{m}$ . The cavity radius is located between the  $\text{H}_2\text{O}$  and  $\text{CO}_2$  snowlines. The disk model parameters are taken from ref.<sup>89</sup>.

and a disk with a deep dust + gas cavity out to 1 au, a location that is in between the two snowlines. The 70 and 200 K contours are also included to highlight the temperature range where  $\text{CO}_2$  is efficiently produced.

If there is no cavity, it is seen that  $\text{H}_2\text{O}$  is highly abundant in the inner disk above the  $\tau_{\text{mid-IR}} = 1$  (where the  $15 \mu\text{m}$  dust continuum becomes optically thick) and would thus produce very strong  $\text{H}_2\text{O}$  lines. However, its column relative to  $\text{CO}_2$  is strongly reduced in the model with a cavity (except at the very edge of the cavity). These models therefore provide a proof of concept for explaining those sources with high  $\text{CO}_2/\text{H}_2\text{O}$  column density ratios with disks that have small cavities.

For the GW Lup disk, the  $\text{H}_2\text{O}$  and  $\text{CO}_2$  snowlines are expected to lie around 0.4 and 1.4 au, respectively<sup>103</sup>, so a qualitatively similar effect can be expected. Such cavities are too small to be resolved with ALMA but could be revealed in their spectral energy distributions or in spectrally resolved CO ro-vibrational line profiles<sup>104–106</sup>. With a few exceptions, these low-mass stars and their disks are generally too weak to image with infrared interferometers<sup>107</sup>.

Interestingly, the strong  $\text{CO}_2$  emission and lack of  $\text{H}_2\text{O}$  in the high-mass source IRAS 23385 also fits into this scenario. The

only difference is that there is not necessarily a cavity but rather a temperature inversion in the inner disk which would cause the  $\text{H}_2\text{O}$ -rich gas to be in absorption (most notably in its  $\nu_2$  band at  $6 \mu\text{m}$ <sup>44</sup>) rather than emission. Figure 7 shows that the temperature in the surface layers in the region where accretional heating no longer dominates (and where lines go back to being in emission), is around 200 K. Such a relatively cool temperature is consistent with that found for the  $\text{CO}_2$  emission in this source (Table 1).

**4.3.2.3 Role of dust traps.** For low-mass sources, a related effect could be the existence of a dust trap triggered by a pressure bump due to a companion that created the cavity. If that dust trap lies between the  $\text{H}_2\text{O}$  and  $\text{CO}_2$  snowlines, it locks up water-rich pebbles thereby suppressing  $\text{H}_2\text{O}$ . However, some gas enriched in carbon<sup>108–110</sup>, or in  $\text{CO}_2$  due to ice sublimation inside its snowline, could still be transported through the trap to the inner disk.

A dust trap locking up the bulk of the  $\text{H}_2\text{O}$  ice would also lower the overall O/H abundance ratio in the inner disk<sup>111</sup>. The same holds for C/H, if CO,  $\text{CH}_4$  and/or carbon-containing molecules are trapped. Some inner disks are indeed known to have low O/H and/or C/H abundances<sup>112–114</sup>. Disks that show spatially resolved dust traps with ALMA<sup>75,115</sup> are likely in this category, provided that the dust traps formed early in the disk’s evolution,



before the bulk of the grains have moved inwards.

In contrast, any disk in which drifting icy pebbles from the outer disk have reached the inner disk and crossed the H<sub>2</sub>O snowline unimpeded should have O/H abundances that could be enhanced by 1–2 orders of magnitude<sup>116,117</sup>. Similarly, CO can be increased in the inner disk due to drifting icy grains<sup>118–120</sup>. Since these icy pebbles are also thought to contain considerable amounts of CO<sub>2</sub> ice, this should not change the relative ratios of the H<sub>2</sub>O and CO<sub>2</sub> lines if both are continuously being supplied to the inner disk<sup>117</sup>, unless the extra CO<sub>2</sub> would remain hidden below the  $\tau_{\text{mid-IR}} = 1$  line due to a lack of vertical mixing. Disks which show compact dust continuum emission with ALMA are good candidates to test this pebble drift scenario.

Figure 8 illustrates these possibilities in a cartoon. It is clear that the combination of large samples of disks studied with both JWST mid-infrared spectroscopy and with ALMA at its highest spatial resolution, including disks that are small and currently unresolved with ALMA at moderate spatial resolution, can provide insight into the relative importance of these processes.

#### 4.3.3 Rich hydrocarbon chemistry: “soot” line and C/O > 1.

The J160532 disk stands out in having unusually strong bands of C<sub>2</sub>H<sub>2</sub> and other hydrocarbons including species that have not been identified in disks before the advent of JWST<sup>1</sup>. Equally interesting is the discovery<sup>1</sup> that the broad bands at 7.7 and 13.7  $\mu\text{m}$  are due to very high column densities of hot C<sub>2</sub>H<sub>2</sub>.

What could be causing such abundant C<sub>2</sub>H<sub>2</sub> in this disk? It is known that PAHs and carbonaceous grains can be destroyed by UV radiation, by chemical processes (e.g., reactions with H, O or OH) or by grain sublimation under the conditions in the inner disk, with C<sub>2</sub>H<sub>2</sub> as a main product<sup>121,122</sup>. When and where the carbon grain sublimation and erosion takes place depends on the type of carbonaceous material. Some laboratory data put the sublimation of amorphous carbon grains at 1200 K<sup>123</sup> whereas other experiments suggest that thermal decomposition of refractory hydrocarbon material (also known as kerogen-like insoluble organic matter, IOM) occurs at lower temperatures, around 400–500 K depending on heating timescale<sup>79,124,125</sup>. This IOM material is thought to make up the bulk of the refractory carbon. Aliphatic and aromatic hydrocarbons, which contain of order 10% of total carbon, sublimate at somewhat lower temperatures of 300–400 K<sup>123</sup>. Together, they form the so-called hydrocarbon “soot” line around 400–500 K, a term coined by Li et al.<sup>79</sup> to indicate the location where the destruction of hydrocarbon solids occurs. This temperature matches well with that found for the high abundance C<sub>2</sub>H<sub>2</sub> gas component. One possibility is therefore that hydrocarbon grain destruction is being observed directly in this disk.

The destruction of carbon grains by thermal processing is thought to be irreversible. On the other hand, the conditions of warm dense gas with high C<sub>2</sub>H<sub>2</sub> abundances are conducive to efficient formation of small aromatic molecules and PAHs up to temperatures where degradation starts to take over<sup>126,127</sup>. Indeed, the production of the smallest aromatic molecule, benzene, in the inner regions of disks as observed here was predicted by Woods & Willacy<sup>69,128</sup>. The J160532 and other similar disks around very

low mass stars<sup>129</sup> are clearly excellent laboratories for studying such hydrocarbon chemistry in detail.

A related interesting question is how common the broad 7.7 and 13.7  $\mu\text{m}$  features indicative of a “soot” line are in other sources. While disks around very low-mass stars are known to have strong C<sub>2</sub>H<sub>2</sub> bands based on *Spitzer* data<sup>49,50,130</sup>, J160532 is the only such disk so far in which the broad bumps are clearly seen. What could make the J160532 disk special? One option is that we are able to look deep into the J160532 disk close to the midplane due to the lack of small grains, as evidenced by the large gas columns and strong H<sub>2</sub> lines<sup>1</sup>. In other disks, the midplane “soot” line could be hidden below the  $\tau_{\text{mid-IR}} = 1$  line. Another option could be that we are witnessing the J160532 disk at a special time when destruction is taking place, perhaps triggered by a recent heating event due to accretion.

The J160532 disk presents another puzzle, namely that of water. The disk is clearly warm enough to sublimate any water ice from the grains and to trigger rapid formation of H<sub>2</sub>O through the reactions of O and OH with H<sub>2</sub>. In disk chemical models, such high abundances of C<sub>2</sub>H<sub>2</sub> compared with H<sub>2</sub>O (Table 2) are only found if the volatile C/O ratio of the gas in the inner disk is significantly increased compared with standard values of volatile C/O = 0.4–0.5. Specifically, C/O ratios > 1 are needed to boost the hydrocarbon production and lock up the bulk of the volatile oxygen in CO and some CO<sub>2</sub><sup>52,63,72</sup>. A small amount of H<sub>2</sub>O could still be produced in the upper layers of the disk where destruction of CO by UV photons or by He<sup>+</sup> frees up some atomic O that can react with H<sub>2</sub> to form H<sub>2</sub>O. Walsh et al.<sup>71</sup> note that the atmospheres of disks around very low mass stars may naturally appear to be carbon rich (without the need for a high C/O ratio) because the unobservable O<sub>2</sub> rather than H<sub>2</sub>O becomes the main gaseous oxygen carrier. However, the orders of magnitude higher C<sub>2</sub>H<sub>2</sub> column and C<sub>2</sub>H<sub>2</sub>/CO<sub>2</sub> ratio observed for J160532 than found in these models strongly points to a genuine carbon-rich atmosphere with C/O > 1.

The most plausible mechanism to lead to C/O > 1 and prevent oxygen from entering the inner disk would be to lock most of it up in water ice in pebbles and planetesimals in the outer disk beyond the water snowline, preventing them from migrating to the inner disk<sup>50,52</sup>, as illustrated in Figure 8 (bottom).

#### 4.3.4 Implications for planet formation

The JWST data provide detailed insight into the chemical composition of the gas in the upper layers of the disk. Planetesimals and planets are, however, formed in the disk midplanes which are not probed directly by mid-infrared data. Nevertheless, indirect information can be obtained if mid-plane material is vertically mixed upward. For example if icy pebbles drift across the water snowline and enhance the gaseous O/H ratio of the midplane gas, this can be mixed upward on comparatively short timescales (e.g., refs.<sup>120,131,132</sup>) to result in enhanced OH and H<sub>2</sub>O emission.

There is also downward gas transport: vertical transport of molecules can be followed by freeze-out onto the colder large grains in the midplane. If those grains become too large to be lifted back up, the disk surface composition becomes part of the planetesimal building material. This so-called “vertical cold fin-

ger effect” also limits the radial extent of the molecular emission: snow surfaces become vertical walls at the midplane snow radius rather than being curved with height in the disk, an effect that is well known for  $\text{H}_2\text{O}$ <sup>81,133,134</sup> but likely also holds for other molecules. Finally, if a gap has opened in a disk, surface layer gas can be accreted directly onto forming giant planets through meridional flows<sup>135,136</sup> thus leaving an imprint on the composition of their atmospheres.

Whether or not carbon-rich planets will be built in the J160532 disk is still an open question and depends also on the time of planet formation. A significant fraction of the carbon is in the gas phase and refractory carbon grains may even have been destroyed in this disk. If this carbon-rich gas were dispersed quickly from the system, only a small fraction of carbon would eventually be included in planets. This scenario has been proposed to explain why Earth is so carbon poor<sup>79,137</sup>.

## 5 Conclusions

The early JWST MIRI-MRS spectra presented here provide examples of how its increased spectral resolution and sensitivity provide new insights into the chemical composition of disks, from young to mature disks and from low- to high-mass stars. In particular, the detection of new species like  $\text{C}_4\text{H}_2$  and  $\text{C}_6\text{H}_6$  allows proposed chemical pathways to be tested. New lines of known species and of their isotopologs, with first detections of  $^{13}\text{CO}_2$  and  $^{13}\text{C}^{12}\text{CH}_2$ , help to break degeneracies between model fit parameters so that their temperatures and column densities can be constrained more accurately. Indeed, orders of magnitude differences in inferred column densities have been found compared with earlier work. The lack of  $\text{NH}_3$  suggests that most of the volatile nitrogen is in unobservable species.

The data highlight the diversity in mid-infrared spectroscopy of disks hinted at by *Spitzer*, from sources dominated by  $\text{CO}_2$  with almost no  $\text{H}_2\text{O}$ , to those rich in  $\text{H}_2\text{O}$  to disks showing booming features of  $\text{C}_2\text{H}_2$ . There are also some similarities: the molecular emission observed in the high-mass protostellar source IRAS 23385, thought to originate from a massive young disk, indicates similar abundance ratios as those found in some  $\text{CO}_2$ -rich low-mass disks.

The diversity in chemistry and spectra is likely related to differences in the physical structures of the disks. Lines are brighter in disks around more luminous sources, which push the emitting area to larger radii and thus boost optically thick lines. The lack or weakness of lines of certain molecules, most notably  $\text{H}_2\text{O}$ , can be due to the very low luminosity of some sources in our sample. However, it is likely also linked to the presence of small cavities in the inner disk that cannot be resolved with ALMA and whose positions extend beyond the water snowline. A related possibility is the presence of dust traps outside of the respective snowlines of different molecules that can lock up certain elements, most notably oxygen, and prevent it from entering the inner disk.

The JWST data also provide evidence for a phenomenon that has been postulated but not seen prior to JWST: the destruction of hydrocarbon grains at the “soot” line boosting the  $\text{C}_2\text{H}_2$  abundance by orders of magnitude<sup>1</sup> and raising the C/O ratio to  $>1$ .

There are a number of obvious next steps in this research. First,

larger samples of disks have to be studied with JWST MIRI-MRS to search for more similarities and probe the limits of diversity, from young to old “debris” disks and across the stellar mass range. MRS spectra of line-rich sources will allow to hunt for other minor species, including  $\text{NH}_3$ . Also, adding NIRSPEC-IFU data for the same sources will be highly valuable to cover the CO ro-vibrational bands at  $4.7\ \mu\text{m}$  as well as the stretching bands of most of the species discussed here. Molecular data on vibration-rotation lines of many molecules, including their isotopologs, are however still incomplete and more laboratory work is needed.

Second, ALMA observations at the highest spatial resolution (down to a few au) are needed to search for small-scale substructure in the continuum that are indicative of dust traps. Their location with respect to different snowlines will help to understand which elements are locked in the outer disk and unable to reach the inner disk. In contrast, some disks may be dominated by drifting icy pebbles that enhance the inner disk in heavy elements. More work is also needed on high resolution studies of the physical structure of high-mass disks with ALMA.

Third, more sophisticated radiative transfer models are needed to analyse the spectra since the current column densities obtained from slab models are only a crude representation of actual abundances and their ratios. Retrieval models using a full 2D temperature and density disk structure but a simplified chemistry is one possibility<sup>138,139</sup>. Retrieval using full chemical models is computationally prohibitive<sup>140</sup>, but such models can then be used as inspiration for abundance distributions and search for trends with physical parameters. In the longer run, full thermo-chemical disk models developed for individual sources can also serve as testbeds for these more simplified approaches. The distribution of small versus large dust and presence of substructures will be a key element in such models.

Finally, the consequences of the observed chemical diversity for the composition of any planets forming in these disks need to be investigated. Ultimately, these disk surveys need to be complemented by JWST surveys of the chemical composition of the atmospheres of mature planets to address the question what sets their composition.

## Author Contributions

Investigation: Grant, Tabone, van Gelder, Francis, Beuther, Bettoni, Gasman, Arabhavi, Nazari, Vlasblom; Writing-original draft: van Dishoeck; Writing-review: all authors; Software: Tabone, Grant, van Gelder, Francis, Arabhavi, Bettoni, Gasman, Klaassen, Christiaens; Visualization: Grant, Nazari, Francis, Vlasblom; Supervision: van Dishoeck, Beuther, Kamp, Henning; Funding: van Dishoeck, Kamp, Henning.

## Conflicts of interest

There are no conflicts to declare.

## Acknowledgements

The authors would like to thank the MIRI GTO JOYS and MINDS teams, as well as the entire MIRI European and US instrument team. Support from StScI is also appreciated. The following National and International Funding Agencies funded and supported

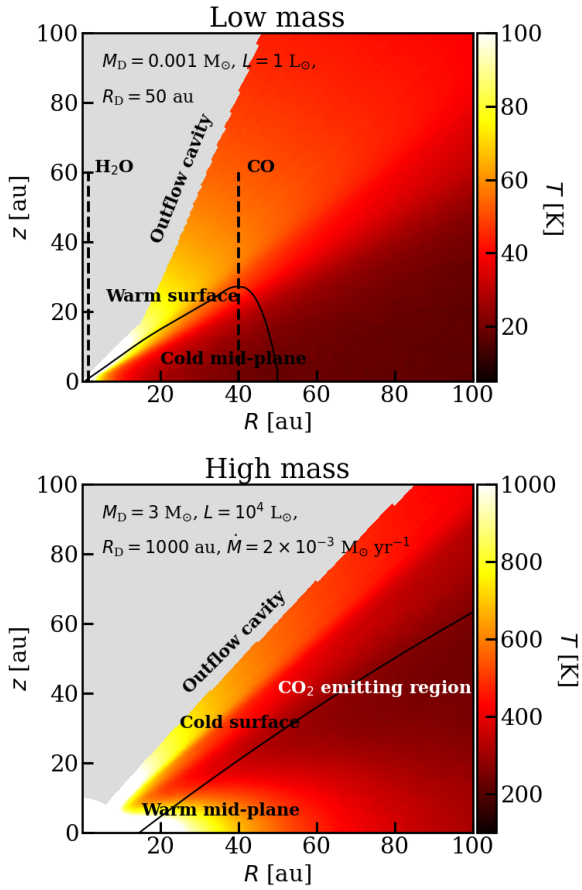


Fig. 7 Two dimensional map of the dust temperature structure of a disk around a low-mass star (top)<sup>86</sup> with that around a high-mass star (bottom)<sup>87</sup>. The solid black line shows the approximate location of the disk, which is still embedded in an envelope for the high-mass source. Note that for the high-mass disk, the midplane temperature in the inner region ( $\leq 50$ –60 au) is larger than that at the disk surface due to accretional heating; no such heating is included for the low-mass source. Such a structure gives rise to mid-infrared absorption lines. At larger radii, the surface is warmer than the midplane due to irradiation resulting in mid-infrared emission lines (indicated with CO<sub>2</sub> emitting region). Model parameters<sup>86,87</sup> are for low mass:  $M_* = 0.5 M_\odot$ ,  $L = 1 L_\odot$ ,  $M_{\text{disk}} = 0.001 M_\odot$ ; high mass:  $M_* = 30 M_\odot$ ,  $L = 10^4 L_\odot$ ,  $M_{\text{disk}} = 3 M_\odot$ ,  $\dot{M} = 2 \times 10^{-3} M_\odot \text{ yr}^{-1}$ . Both models use dust opacities appropriate for large grains<sup>86</sup>. For the low-mass disk, the H<sub>2</sub>O snowline is at 1.5 au and the CO snowline at 40 au; for the high-mass disk, they are at 390 au and >20000 au, respectively.

the MIRI development: NASA; ESA; Belgian Science Policy Office (BELSPO); Centre Nationale d’Etudes Spatiales (CNES); Danish National Space Centre; Deutsches Zentrum für Luftund Raumfahrt (DLR); Enterprise Ireland; Ministerio De Economía y Competividad; Netherlands Research School for Astronomy (NOVA); Netherlands Organisation for Scientific Research (NWO); Science and Technology Facilities Council; Swiss Space Office; Swedish National Space Agency; and UK Space Agency.

EvD acknowledges support from ERC Advanced grant 101019751 MOLDISK, the Danish National Research Foundation through the Center of Excellence “InterCat” (DNRF150), and DFG-grant 325594231, FOR 2634/2. BT is a Laureate

of the Paris Region fellowship program, which is supported by the Ile-de-France Region and has received funding under Marie Skłodowska-Curie grant agreement No. 945298. DG thanks the Research Foundation Flanders for co-financing the present research (grant number V435622N). TH is grateful for support from the ERC Advanced grant 832428 Origins; IK, MvG, LF, AA and EvD from TOP-1 grant 614.001.751 from the Dutch Research Council (NWO); and IK from H2020-MSCA-ITN- 2019, grant no. 860470 (CHAMELEON).

## Notes and references

- 1 B. Tabone, G. Bettoni, E. F. van Dishoeck, A. M. Arabhavi, S. Grant, D. Gasman, T. Henning, I. Kamp, M. Güdel, P. O. Lagage, T. Ray, B. Vandenbussche, A. Abergel, O. Absil, I. Argyriou, D. Barrado, A. Boccaletti, J. Bouwman, A. Caratti o Garatti, V. Geers, A. M. Glauser, K. Justannont, F. Lahuis, M. Mueller, C. Nehmé, G. Olofsson, E. Pantin, S. Scheithauer, C. Waelkens, L. B. F. M. Waters, J. H. Black, V. Christiaens, R. Guadarrama, M. Morales-Calderón, H. Jang, J. Kanwar, N. Pawellek, G. Perotti, A. Perrin, D. Rodgers-Lee, M. Samsland, J. Schreiber, K. Schwarz, L. Colina, G. Östlin and G. Wright, *Nature Astronomy*, 2023.
- 2 K. I. Öberg and E. A. Bergin, *Phys. Rep.*, 2021, **893**, 1–48.
- 3 E. F. van Dishoeck and E. A. Bergin, *ExoFrontiers; Big Questions in Exoplanetary Science*, IOP, Bristol, UK, 2021, pp. 14–1.
- 4 A. Miotello, I. Kamp, T. Birnstiel, L. I. Cleeves and A. Kataoka, *arXiv e-prints*, 2022, arXiv:2203.09818.
- 5 M. L. R. van’t Hoff, D. Harsono, J. J. Tobin, A. D. Bosman, E. F. van Dishoeck, J. K. Jørgensen, A. Miotello, N. M. Murillo and C. Walsh, *Astrophys. J.*, 2020, **901**, 166.
- 6 Ł. Tychoniec, C. F. Manara, G. P. Rosotti, E. F. van Dishoeck, A. J. Cridland, T.-H. Hsieh, N. M. Murillo, D. Segura-Cox, S. E. van Terwisga and J. J. Tobin, *Astron. Astrophys.*, 2020, **640**, A19.
- 7 A. Morbidelli, J. I. Lunine, D. P. O’Brien, S. N. Raymond and K. J. Walsh, *Annual Review of Earth and Planetary Sciences*, 2012, **40**, 251–275.
- 8 R. I. Dawson and J. A. Johnson, *Annu. Rev. Astron. Astrophys.*, 2018, **56**, 175–221.
- 9 J. S. Carr and J. R. Najita, *Science*, 2008, **319**, 1504.
- 10 C. Salyk, K. M. Pontoppidan, G. A. Blake, J. R. Najita and J. S. Carr, *Astrophys. J.*, 2011, **731**, 130.
- 11 K. M. Pontoppidan, C. Salyk, E. A. Bergin, S. Brittain, B. Marty, O. Mousis and K. L. Oberg, in *Protostars & Planets VI*, ed. Beuther, H., Klessen, R., Dullemond, K., Henning, Th., Tucson: Univ. Arizona Press, 2014, pp. 363–385.
- 12 L. I. Cleeves, *IAU Symposium*, 2018, **332**, 57–68.
- 13 K. I. Öberg, V. V. Guzmán, C. Walsh, Y. Aikawa, E. A. Bergin, C. J. Law, R. A. Loomis, F. Alarcón, S. M. Andrews, J. Bae, J. B. Bergner, Y. Boehler, A. S. Booth, A. D. Bosman, J. K. Calahan, G. Cataldi, L. I. Cleeves, I. Czekala, K. Furuya, J. Huang, J. D. Ilee, N. T. Kurtovic, R. Le Gal, Y. Liu, F. Long, F. Ménard, H. Nomura, L. M. Pérez, C. Qi, K. R. Schwarz, A. Sierra, R. Teague, T. Tsukagoshi, Y. Yamato, M. L. R. van’t

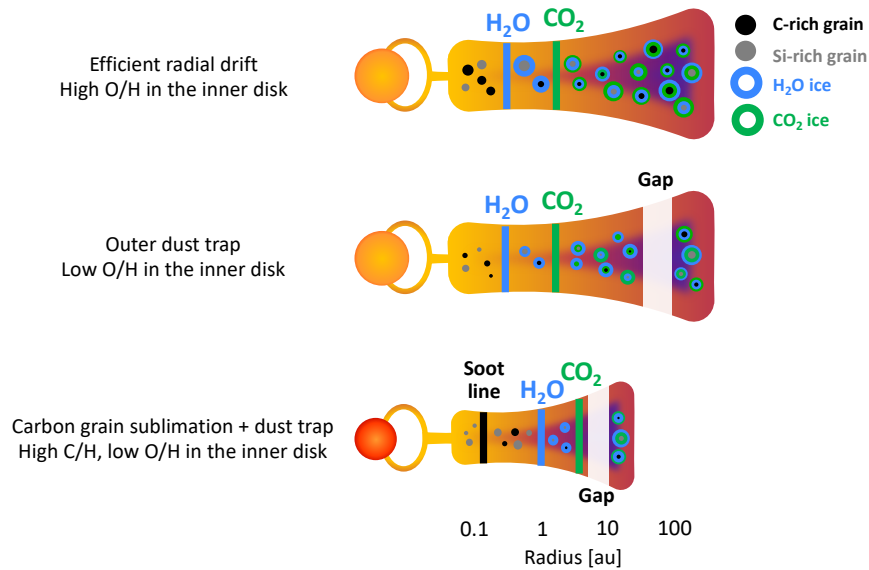


Fig. 8 Cartoons illustrating the cases of (a) enhanced H<sub>2</sub>O and O/H in the inner disk due to icy pebble drift; (b) reduced H<sub>2</sub>O and O/H in the inner disk due to a dust trap outside the H<sub>2</sub>O snowline. If this trap is still inside the CO<sub>2</sub> snowline, CO<sub>2</sub> could be enhanced; and (c) as (b) but for a very low-mass star with enhanced C<sub>2</sub>H<sub>2</sub> at the soot line.

- Hoff, A. R. Waggoner, D. J. Wilner and K. Zhang, *Astrophys. J. Suppl. Ser.*, 2021, **257**, 1.
- 14 M. Wells, J. W. Pel, A. Glasse, G. S. Wright, G. Aitink-Kroes, R. Azzollini, S. Beard, B. R. Brandl, A. Gallie, V. C. Geers, A. M. Glauser, P. Hastings, T. Henning, R. Jager, K. Justtanont, B. Kruizinga, F. Lahuis, D. Lee, I. Martinez-Delgado, J. R. Martínez-Galarza, M. Meijers, J. E. Morrison, F. Müller, T. Nakos, B. O’Sullivan, A. Oudenhuysen, P. Parr-Burman, E. Pauwels, R. R. Rohloff, E. Schmalzl, J. Sykes, M. P. Thelen, E. F. van Dishoeck, B. Vandenbussche, L. B. Venema, H. Visser, L. B. F. M. Waters and D. Wright, *Publ. Astron. Soc. Pac.*, 2015, **127**, 646.
- 15 G. H. Rieke, G. S. Wright, T. Böker, J. Bouwman, L. Colina, A. Glasse, K. D. Gordon, T. P. Greene, M. Güdel, T. Henning, K. Justtanont, P. O. Lagage, M. E. Meixner, H. U. Nørgaard-Nielsen, T. P. Ray, M. E. Ressler, E. F. van Dishoeck and C. Waelkens, *Publ. Astron. Soc. Pac.*, 2015, **127**, 584.
- 16 G. S. Wright, G. H. Rieke, A. Glasse, M. Ressler, M. García Marín, J. Aguilar, S. Alberts, J. Álvarez-Márquez, I. Argyriou, K. Banks, P. Baudoz, A. Boccaletti, P. Bouchet, J. Bouwman, B. R. Brandl, D. Breda, S. Bright, S. Cale, L. Colina, C. Cosso, A. Coulais, M. Cracraft, W. De Meester, D. Dicken, M. Engesser, M. Etxaluze, O. D. Fox, S. Friedman, H. Fu, D. Gasman, A. Gáspár, R. Gastaud, V. Geers, A. M. Glauser, K. D. Gordon, T. Greene, T. R. Greve, T. Grundy, M. Güdel, P. Guillard, P. Haderlein, R. Hashimoto, T. Henning, D. Hines, B. Holler, Ö. H. Detre, A. Jahromi, B. James, O. C. Jones, K. Justtanont, P. Kavanagh, S. Kendrew, P. Klaassen, O. Krause, A. Labiano, P.-O. Lagage, S. Lambros, K. Larson, D. Law, D. Lee, M. Libralato, J. Lorenzo Alvarez, M. Meixner, J. Morrison, M. Mueller, K. Murray, M. Mycroft, R. Myers, O. Nayak, B. Naylor, B. Nickson, A. Noriega-Crespo, G. Östlin, B. O’Sullivan, R. Ottens, P. Patapis, K. Penanen, M. Pietraszkiwicz, T. Ray, M. Regan, A. Roteliuk, P. Royer, P. Samara-Ratna, B. Samuelson, B. A. Sargent, S. Scheithauer, A. Schneider, J. Schreiber, B. Shaughnessy, E. Sheehan, I. Shivaie, G. C. Sloan, L. Tamas, K. Teague, T. Temim, T. Tikkanen, S. Tustain, E. F. van Dishoeck, B. Vandenbussche, M. Weilert, P. Whitehouse and S. Wolff, *Publ. Astron. Soc. Pac.*, 2023, **135**, 048003.
- 17 E. van Dishoeck, and et al., *A&A*, *in prep.*, 2023.
- 18 I. Kamp, and et al., *Faraday Discussions*, 2023.
- 19 T. Henning, and et al., *PASP*, *in prep.*, 2023.
- 20 R. Cesaroni, H. Beuther, A. Ahmadi, M. T. Beltrán, T. Csengeri, R. Galván-Madrid, C. Gieser, T. Henning, K. G. Johnston, P. D. Klaassen, R. Kuiper, S. Leurini, H. Linz, S. Longmore, S. L. Lumsden, L. T. Maud, L. Moscadelli, J. C. Mottram, A. Palau, T. Peters, R. E. Pudritz, Á. Sánchez-Monge, P. Schilke, D. Semenov, S. Suri, J. S. Urquhart, J. M. Winters, Q. Zhang and H. Zinnecker, *Astron. Astrophys.*, 2019, **627**, A68.
- 21 S. Molinari, L. Testi, J. Brand, R. Cesaroni and F. Palla, *Astrophys. J. Lett.*, 1998, **505**, L39–L42.
- 22 H. Beuther, J. C. Mottram, A. Ahmadi, F. Bosco, H. Linz, T. Henning, P. Klaassen, J. M. Winters, L. T. Maud, R. Kuiper, D. Semenov, C. Gieser, T. Peters, J. S. Urquhart, R. Pudritz, S. E. Ragan, S. Feng, E. Keto, S. Leurini, R. Cesaroni, M. Beltran, A. Palau, Á. Sánchez-Monge, R. Galvan-Madrid, Q. Zhang, P. Schilke, F. Wyrowski, K. G. Johnston, S. N. Longmore, S. Lumsden, M. Hoare, K. M. Menten and T. Csengeri, *Astron. Astrophys.*, 2018, **617**, A100.
- 23 F. Faustini, S. Molinari, L. Testi and J. Brand, *Astron. Astrophys.*, 2009, **503**, 801–816.
- 24 J. M. Alcalá, C. F. Manara, A. Natta, A. Frasca, L. Testi,

- B. Nisini, B. Stelzer, J. P. Williams, S. Antonucci, K. Biazzo, E. Covino, M. Esposito, F. Getman and E. Rigliaco, *Astron. Astrophys.*, 2017, **600**, A20.
- 25 K. L. Luhman, K. A. Herrmann, E. E. Mamajek, T. L. Esplin and M. J. Pecaut, *Astron. J.*, 2018, **156**, 76.
- 26 Gaia Collaboration, A. Vallenari, A. G. A. Brown, T. Prusti, J. H. J. de Bruijne, F. Arenou, C. Babusiaux, M. Biermann, O. L. Creevey, C. Ducourant, D. W. Evans, L. Eyer, R. Guerra, A. Hutton, C. Jordi, S. A. Klioner, U. L. Lammers, L. Lindgren, X. Luri, F. Mignard, C. Panem, D. Pourbaix, S. Randich, P. Sartoretti, C. Soubiran, P. Tanga, N. A. Walton, C. A. L. Bailer-Jones, U. Bastian, R. Drimmel, F. Jansen, D. Katz, M. G. Lattanzi, F. van Leeuwen, J. Bakker, C. Cacciari, J. Castañeda, F. De Angeli, C. Fabricius, M. Fouesneau, Y. Frémat, L. Galluccio, A. Guerrier, U. Heiter, E. Masana, R. Messineo, N. Mowlavi, C. Nicolas, K. Nienartowicz, F. Pailler, P. Panuzzo, F. Riclet, W. Roux, G. M. Seabroke, R. Sordoørcit, F. Thévenin, G. Gracia-Abril, J. Portell, D. Teyssier, M. Altmann, R. Andrae, M. Audard, I. Bellas-Velidis, K. Benson, J. Berthier, R. Blomme, P. W. Burgess, D. Busonero, G. Busso, H. Cánovas, B. Carry, A. Cellino, N. Cheek, G. Clementini, Y. Damerdj, M. Davidson, P. de Teodoro, M. Nuñez Campos, L. Delchambre, A. Dell’Oro, P. Esquej, J. Fernández-Hernández, E. Fraile, D. Garabato, P. García-Lario, E. Gosset, R. Haigron, J. L. Halbwachs, N. C. Hambly, D. L. Harrison, J. Hernández, D. Hestroffer, S. T. Hodgkin, B. Holl, K. Janßen, G. Jevardat de Fombelle, S. Jordan, A. Krone-Martins, A. C. Lanzafame, W. Löffler, O. Marchal, P. M. Marrese, A. Moitinho, K. Muinonen, P. Osborne, E. Pancino, T. Pauwels, A. Recio-Blanco, C. Reylé, M. Riello, L. Rimoldini, T. Roegiers, J. Rybizki, L. M. Sarro, C. Siopis, M. Smith, A. Sozzetti, E. Utrilla, M. van Leeuwen, U. Abbas, P. Abraham, A. Abreu Aramburu, C. Aerts, J. J. Aguado, M. Ajaj, F. Aldea-Montero, G. Altavilla, M. A. Álvarez, J. Alves, F. Anders, R. I. Anderson, E. Anglada Varela, T. Antoja, D. Baines, S. G. Baker, L. Balaguer-Núñez, E. Balbinot, Z. Balog, C. Barache, D. Barbato, M. Barros, M. A. Barstow, S. Bartolomé, J. L. Bassilana, N. Bauchet, U. Beciani, M. Bellazzini, A. Berihuete, M. Bernet, S. Bertone, L. Bianchi, A. Binnenfeld, S. Blanco-Cuaresma, A. Blazere, T. Boch, A. Bombrun, D. Bossini, S. Bouquillon, A. Bragaglia, L. Bramante, E. Breedt, A. Bressan, N. Brouillet, E. Brugaletta, B. Bucciarelli, A. Burlacu, A. G. Butkevich, R. Buzz, E. Caffau, R. Cancelliere, T. Cantat-Gaudin, R. Carballo, T. Carlucci, M. I. Carnerero, J. M. Carrasco, L. Casamiquela, M. Castellani, A. Castro-Ginard, L. Chaoul, P. Charlot, L. Chemin, V. Chiaramida, A. Chiavassa, N. Chornay, G. Comoretto, G. Contursi, W. J. Cooper, T. Cornez, S. Cowell, F. Crifo, M. Cropper, M. Crosta, C. Crowley, C. Dafonte, A. Dapergolas, M. David, P. David, P. de Laverny, F. De Luise, R. De March, J. De Ridder, R. de Souza, A. de Torres, E. F. del Peloso, E. del Pozo, M. Delbo, A. Delgado, J. B. Delisle, C. Demouchy, T. E. Dharmawardena, P. Di Matteo, S. Diakite, C. Diener, E. Distefano, C. Dolding, B. Edvardsson, H. Enke, C. Fabre, M. Fabrizio, S. Faigler, G. Fedorets, P. Fernique, A. Fienga, F. Figueras, Y. Fournier, C. Fouron, F. Fragkoudi, M. Gai, A. Garcia-Gutierrez, M. Garcia-Reinaldos, M. García-Torres, A. Garofalo, A. Gavel, P. Gavras, E. Gerlach, R. Geyer, P. Giacobbe, G. Gilmore, S. Girona, G. Giuffrida, R. Gomel, A. Gomez, J. González-Núñez, I. González-Santamaría, J. J. González-Vidal, M. Granvik, P. Guillout, J. Guiraud, R. Gutiérrez-Sánchez, L. P. Guy, D. Hatzidimitriou, M. Hauser, M. Haywood, A. Helmer, A. Helmi, M. H. Sarmiento, S. L. Hidalgo, T. Hilger, N. Hładczuk, D. Hobbs, G. Holland, H. E. Huckle, K. Jardine, G. Jasniewicz, A. Jean-Antoine Piccolo, Ó. Jiménez-Arranz, A. Jorissen, J. Juaristi Campillo, F. Julbe, L. Karbevská, P. Kervella, S. Khanna, M. Kontizas, G. Kordopatis, A. J. Korn, Á. Kóspál, Z. Kostrzewa-Rutkowska, K. Kruszyńska, M. Kun, P. Laizeau, S. Lambert, A. F. Lanza, Y. Lasne, J. F. Le Campion, Y. Lebreton, T. Lebzelter, S. Leccia, N. Leclerc, I. Lecoœur-Taïbi, S. Liao, E. L. Licata, H. E. P. Lindstrøm, T. A. Lister, E. Livanou, A. Lobel, A. Lorca, C. Loup, P. Madrero Pardo, A. Magdaleno Romeo, S. Managau, R. G. Mann, M. Mantega, J. M. Marchant, M. Marconi, J. Marcos, M. M. S. Marcos Santos, D. Marín Pina, S. Marinoni, F. Marocco, D. J. Marshall, L. M. Polo, J. M. Martín-Fleitas, G. Marton, N. Mary, A. Masip, D. Massari, A. Mastrobuono-Battisti, T. Mazeh, P. J. McMillan, S. Messina, D. Michalik, N. R. Millar, A. Mints, D. Molina, R. Molinaro, L. Molnár, G. Monari, M. Monguió, P. Montegriffo, A. Montero, R. Mor, A. Mora, R. Morbidelli, T. Morel, D. Morris, T. Muraveva, C. P. Murphy, I. Musella, Z. Nagy, L. Noval, F. Ocaña, A. Ogden, C. Ordenovic, J. O. Osinde, C. Pagani, I. Pagano, L. Palaversa, P. A. Palicio, L. Pallas-Quintela, A. Panahi, S. Payne-Wardenaar, X. Peñalosa Esteller, A. Penttilä, B. Pichon, A. M. Piersimoni, F. X. Pineau, E. Plachy, G. Plum, E. Poggio, A. Prša, L. Pulonge, E. Racero, S. Ragaini, M. Rainer, C. M. Raiteri, N. Rambaux, P. Ramos, M. Ramos-Lerate, P. Re Fiorentin, S. Regibo, P. J. Richards, C. Rios Diaz, V. Ripepi, A. Riva, H. W. Rix, G. Rixon, N. Robichon, A. C. Robin, C. Robin, M. Roelens, H. R. O. Rogues, L. Rohrbasser, M. Romero-Gómez, N. Rowell, F. Royer, D. Ruz Mieres, K. A. Rybicki, G. Sadowski, A. Sáez Núñez, A. Sagristà Sellés, J. Sahlmann, E. Salguero, N. Samaras, V. Sanchez Gimenez, N. Sanna, R. Santoveña, M. Sarasso, M. Schultheis, E. Sciacca, M. Segol, J. C. Segovia, D. Ségransan, D. Semeux, S. Shahaf, H. I. Siddiqui, A. Siebert, L. Siltala, A. Silvelo, E. Slezak, I. Slezak, R. L. Smart, O. N. Snaith, E. Solano, F. Solitro, D. Souami, J. Souchay, A. Spagna, L. Spina, F. Spoto, I. A. Steele, H. Steidelmüller, C. A. Stephenson, M. Süveges, J. Surdej, L. Szabados, E. Szegedi-Elek, F. Taris, M. B. Taylo, R. Teixeira, L. Tolomei, N. Tonello, F. Torra, J. Torra, G. Torralba Elipse, M. Trabucchi, A. T. Tsounis, C. Turon, A. Ulla, N. Unger, M. V. Vaillant, E. van Dillen, W. van Reeve, O. Vanel, A. Vecchiato, Y. Viala, D. Vicente, S. Voutsinas, M. Weiler, T. Wevers, L. Wyrzykowski, A. Yoldas, P. Yvard, H. Zhao, J. Zorec, S. Zucker and T. Zwitter, *arXiv e-prints*, 2022, arXiv:2208.00211.
- 27 N. Miret-Roig, P. A. B. Galli, J. Olivares, H. Bouy, J. Alves

- and D. Barrado, *Astron. Astrophys.*, 2022, **667**, A163.
- 28 H. Bushouse, J. Eisenhamer, N. Dencheva, J. Davies, P. Greenfield, J. Morrison, P. Hodge, B. Simon, D. Grumm, M. Droettboom, E. Slavich, M. Sosey, T. Pauly, T. Miller, R. Jedrzejewski, W. Hack, D. Davis, S. Crawford, D. Law, K. Gordon, M. Regan, M. Cara, K. MacDonald, L. Bradley, C. Shanahan and W. Jamieson, *spacetelescope/jwst: JWST 1.6.2*, Zenodo, 2022.
  - 29 D. Gasman, I. Argyriou, G. C. Sloan, B. Aringer, J. Álvarez-Márquez, O. Fox, A. Glasse, A. Glauser, O. C. Jones, K. Justtanont, P. J. Kavanagh, P. Klaassen, A. Labiano, K. Larson, D. R. Law, M. Mueller, O. Nayak, A. Noriega-Crespo, P. Patapis, P. Royer and B. Vandenbussche, *Astron. Astrophys.*, 2023, **673**, A102.
  - 30 H. Beuther, E. F. van Dishoeck, L. Tychoniec, C. Gieser, P. J. Kavanagh, G. Perotti, M. L. van Gelder, P. Klaassen, A. Caratti o Garatti, L. Francis, W. R. M. Rocha, K. Slavicsinska, T. Ray, K. Justtanont, H. Linnartz, C. Waelkens, L. Colina, T. Greve, M. Güdel, T. Henning, P. O. Lagage, B. Vandenbussche, G. Östlin and G. Wright, *Astron. Astrophys.*, 2023, **673**, A121.
  - 31 S. L. Grant, E. F. van Dishoeck, B. Tabone, D. Gasman, T. Henning, I. Kamp, M. Güdel, P.-O. Lagage, G. Bettoni, G. Perotti, V. Christiaens, M. Samland, A. M. Arabhavi, I. Argyriou, A. Abergel, O. Absil, D. Barrado, A. Boccaletti, J. Bouwman, A. C. o. Garatti, V. Geers, A. M. Glauser, R. Guadarrama, H. Jang, J. Kanwar, F. Lahuis, M. Morales-Calderón, M. Mueller, C. Nehmé, G. Olofsson, E. Pantin, N. Pawellek, T. P. Ray, D. Rodgers-Lee, S. Scheithauer, J. Schreiber, K. Schwarz, M. Temmink, B. Vandenbussche, M. Vlasblom, L. B. F. M. Waters, G. Wright, L. Colina, T. R. Greve, K. Justannont and G. Östlin, *arXiv e-prints*, 2022, arXiv:2212.08047.
  - 32 J. S. Carr and J. R. Najita, *Astrophys. J.*, 2011, **733**, 102.
  - 33 S. Bruderer, D. Harsono and E. F. van Dishoeck, *Astron. Astrophys.*, 2015, **575**, A94.
  - 34 I. Gordon, L. Rothman, R. Hargreaves, R. Hashemi, E. Karlovets, F. Skinner, E. Conway, C. Hill, R. Kochanov, Y. Tan, P. Wcisło, A. Finenko, K. Nelson, P. Bernath, M. Birk, V. Boudon, A. Campargue, K. Chance, A. Coustenis, B. Drouin, J. Flaud, R. Gamache, J. Hodges, D. Jacquemart, E. Mlawer, A. Nikitin, V. Perevalov, M. Rotger, J. Tennyson, G. Toon, H. Tran, V. Tyuterev, E. Adkins, A. Baker, A. Barbe, E. Canè, A. Császár, A. Dudaryonok, O. Egorov, A. Fleisher, H. Fleurbaey, A. Foltynowicz, T. Furtenbacher, J. Harrison, J. Hartmann, V. Horneman, X. Huang, T. Karman, J. Karns, S. Kass, I. Kleiner, V. Kofman, F. Kwabia-Tchana, N. Lavrentieva, T. Lee, D. Long, A. Lukashchuk, O. Lyulin, V. Makhnev, W. Matt, S. Massie, M. Melosso, S. Mikhailenko, D. Mondelain, H. Müller, O. Naumenko, A. Perrin, O. Polyansky, E. Raddaoui, P. Raston, Z. Reed, M. Rey, C. Richard, R. Tóbiás, I. Sadiek, D. Schwenke, E. Starikova, K. Sung, F. Tamassia, S. Tashkun, J. Vander Auwera, I. Vasilenko, A. Vigan, G. Villanueva, B. Vispoel, G. Wagner, A. Yachmenev and S. Yurchenko, *Journal of Quantitative Spectroscopy and Radiative Transfer*, 2022, **277**, 107949.
  - 35 F. F. S. van der Tak, F. Lique, A. Faure, J. H. Black and E. F. van Dishoeck, *Atoms*, 2020, **8**, 15.
  - 36 T. Delahaye, R. Armante, N. Scott, N. Jacquinet-Husson, A. Chédin, L. Crépeau, C. Crevoisier, V. Douet, A. Perrin, A. Barbe, V. Boudon, A. Campargue, L. Coudert, V. Ebert, J.-M. Flaud, R. Gamache, D. Jacquemart, A. Jolly, F. Kwabia Tchana, A. Kyuberis, G. Li, O. Lyulin, L. Manceron, S. Mikhailenko, N. Moazzen-Ahmadi, H. Müller, O. Naumenko, A. Nikitin, V. Perevalov, C. Richard, E. Starikova, S. Tashkun, V. Tyuterev, J. Vander Auwera, B. Vispoel, A. Yachmenev and S. Yurchenko, *Journal of Molecular Spectroscopy*, 2021, **380**, 111510.
  - 37 A. Labiano, I. Argyriou, J. Álvarez-Márquez, A. Glasse, A. Glauser, P. Patapis, D. Law, B. R. Brandl, K. Justtanont, F. Lahuis, J. R. Martínez-Galarza, M. Mueller, A. Noriega-Crespo, P. Royer, B. Shaughnessy and B. Vandenbussche, *Astron. Astrophys.*, 2021, **656**, A57.
  - 38 E. L. Gibb, D. C. B. Whittet, A. C. A. Boogert and A. G. G. M. Tielens, *Astrophys. J. Suppl. Ser.*, 2004, **151**, 35–73.
  - 39 F. C. Adams, C. J. Lada and F. H. Shu, *Astrophys. J.*, 1987, **312**, 788.
  - 40 E. L. Gibb, D. C. B. Whittet, W. A. Schutte, A. C. A. Boogert, J. E. Chiar, P. Ehrenfreund, P. A. Gerakines, J. V. Keane, A. G. G. M. Tielens, E. F. van Dishoeck and O. Kerkhof, *Astrophys. J.*, 2000, **536**, 347–356.
  - 41 A. C. A. Boogert, P. A. Gerakines and D. C. B. Whittet, *Annu. Rev. Astron. Astrophys.*, 2015, **53**, 541–581.
  - 42 Molinari, S., Faustini, F., Testi, L., Pezzuto, S., Cesaroni, R. and Brand, J., *A&A*, 2008, **487**, 1119–1128.
  - 43 C. Gieser, and et al., *A&A subm.*, 2023.
  - 44 L. Francis, and et al., *A&A in prep.*, 2023.
  - 45 D. Gasman, E. F. van Dishoeck, S. L. Grant, M. Temmink, B. Tabone, T. Henning, I. Kamp, M. Güdel, P.-O. Lagage, G. Perotti, V. Christiaens, M. Samland, A. M. Arabhavi, I. Argyriou, A. Abergel, O. Absil, D. Barrado, A. Boccaletti, J. Bouwman, A. C. o. Garatti, V. Geers, A. M. Glauser, R. Guadarrama, H. Jang, J. Kanwar, F. Lahuis, M. Morales-Calderón, M. Mueller, C. Nehmé, G. Olofsson, E. Pantin, N. Pawellek, T. P. Ray, D. Rodgers-Lee, S. Scheithauer, J. Schreiber, K. Schwarz, B. Vandenbussche, M. Vlasblom, L. B. F. M. Waters, G. Wright, L. Colina, T. R. Greve and G. Östlin, *arXiv e-prints*, 2023, arXiv:2307.09301.
  - 46 J. Kessler-Silacci, J.-C. Augereau, C. P. Dullemond, V. Geers, F. Lahuis, I. Evans, Neal J., E. F. van Dishoeck, G. A. Blake, A. C. A. Boogert, J. Brown, J. K. Jørgensen, C. Knez and K. M. Pontoppidan, *Astrophys. J.*, 2006, **639**, 275–291.
  - 47 E. Furlan, L. Hartmann, N. Calvet, P. D'Alessio, R. Franco-Hernández, W. J. Forrest, D. M. Watson, K. I. Uchida, B. Sargent, J. D. Green, L. D. Keller and T. L. Herter, *Astrophys. J. Suppl. Ser.*, 2006, **165**, 568–605.
  - 48 T. Henning, *Annu. Rev. Astron. Astrophys.*, 2010, **48**, 21–46.
  - 49 S. E. Dahm and J. M. Carpenter, *Astron. J.*, 2009, **137**, 4024–4045.

- 50 I. Pascucci, G. Herczeg, J. S. Carr and S. Bruderer, *Astrophys. J.*, 2013, **779**, 178.
- 51 V. C. Geers, J. C. Augereau, K. M. Pontoppidan, C. P. Dullemond, R. Visser, J. E. Kessler-Silacci, I. Evans, N. J., E. F. van Dishoeck, G. A. Blake, A. C. A. Boogert, J. M. Brown, F. Lahuis and B. Merín, *Astron. Astrophys.*, 2006, **459**, 545–556.
- 52 J. R. Najita, J. S. Carr, K. M. Pontoppidan, C. Salyk, E. F. van Dishoeck and G. A. Blake, *Astrophys. J.*, 2013, **766**, 134.
- 53 K. M. Pontoppidan, C. Salyk, A. Banzatti, G. A. Blake, C. Walsh, J. H. Lacy and M. J. Richter, *Astrophys. J.*, 2019, **874**, 92.
- 54 F. P. Helmich, E. F. van Dishoeck, J. H. Black, T. de Graauw, D. A. Beintema, A. M. Heras, F. Lahuis, P. W. Morris and E. A. Valentijn, *Astron. Astrophys.*, 1996, **315**, L173–L176.
- 55 F. Lahuis and E. F. van Dishoeck, *Astron. Astrophys.*, 2000, **355**, 699–712.
- 56 A. M. S. Boonman, E. F. van Dishoeck, F. Lahuis and S. D. Doty, *Astron. Astrophys.*, 2003, **399**, 1063–1072.
- 57 C. Knez, J. H. Lacy, I. Evans, Neal J., E. F. van Dishoeck and M. J. Richter, *Astrophys. J.*, 2009, **696**, 471–483.
- 58 A. G. Barr, A. Boogert, C. N. DeWitt, E. Montiel, M. J. Richter, J. H. Lacy, D. A. Neufeld, N. Indriolo, Y. Pendleton, J. Chiar and A. G. G. M. Tielens, *Astrophys. J.*, 2020, **900**, 104.
- 59 A. M. S. Boonman, E. F. van Dishoeck, F. Lahuis, S. D. Doty, C. M. Wright and D. Rosenthal, *Astron. Astrophys.*, 2003, **399**, 1047–1061.
- 60 P. Sonnentrucker, E. González-Alfonso, D. A. Neufeld, E. A. Bergin, G. J. Melnick, W. J. Forrest, J. L. Pipher and D. M. Watson, *Astrophys. J. Lett.*, 2006, **650**, L71–L74.
- 61 P. Sonnentrucker, E. González-Alfonso and D. A. Neufeld, *Astrophys. J. Lett.*, 2007, **671**, L37–L40.
- 62 E. F. van Dishoeck, L. E. Kristensen, J. C. Mottram, A. O. Benz, E. A. Bergin, P. Caselli, F. Herpin, M. R. Hogerheijde, D. Johnstone, R. Liseau, B. Nisini, M. Tafalla, F. F. S. van der Tak, F. Wyrowski, A. Baudry, M. Benedettini, P. Bjerkeli, G. A. Blake, J. Braine, S. Bruderer, S. Cabrit, J. Cernicharo, Y. Choi, A. Coutens, T. de Graauw, C. Dominik, D. Fedele, M. Fich, A. Fuente, K. Furuya, J. R. Goicoechea, D. Harsono, F. P. Helmich, G. J. Herczeg, T. Jacq, A. Karska, M. Kaufman, E. Keto, T. Lamberts, B. Larsson, S. Leurini, D. C. Lis, G. Melnick, D. Neufeld, L. Pagani, M. Persson, R. Shipman, V. Taquet, T. A. van Kempen, C. Walsh, S. F. Wampfler, U. Yildiz and WISH Team, *Astron. Astrophys.*, 2021, **648**, A24.
- 63 P. Woitke, M. Min, W. F. Thi, C. Roberts, A. Carmona, I. Kamp, F. Ménard and C. Pinte, *Astron. Astrophys.*, 2018, **618**, A57.
- 64 E. F. van Dishoeck, *Proc. Natl Acad. Sci. USA*, 2006, **103**, 12249–12256.
- 65 P. Woitke, I. Kamp and W.-F. Thi, *Astron. Astrophys.*, 2009, **501**, 383–406.
- 66 S. Bruderer, E. F. van Dishoeck, S. D. Doty and G. J. Herczeg, *Astron. Astrophys.*, 2012, **541**, A91.
- 67 C. Walsh, H. Nomura, T. J. Millar and Y. Aikawa, *Astrophys. J.*, 2012, **747**, 114.
- 68 M. Agúndez, J. Cernicharo and J. R. Goicoechea, *Astron. Astrophys.*, 2008, **483**, 831–837.
- 69 P. M. Woods and K. Willacy, *Astrophys. J.*, 2009, **693**, 1360–1378.
- 70 A. E. Glassgold, R. Meijerink and J. R. Najita, *Astrophys. J.*, 2009, **701**, 142–153.
- 71 C. Walsh, H. Nomura and E. van Dishoeck, *Astron. Astrophys.*, 2015, **582**, A88.
- 72 D. E. Anderson, G. A. Blake, L. I. Cleeves, E. A. Bergin, K. Zhang, K. R. Schwarz, C. Salyk and A. D. Bosman, *Astrophys. J.*, 2021, **909**, 55.
- 73 K. I. Öberg, R. Murray-Clay and E. A. Bergin, *Astrophys. J. Lett.*, 2011, **743**, L16.
- 74 S. E. Bisschop, H. J. Fraser, K. I. Öberg, E. F. van Dishoeck and S. Schlemmer, *Astron. Astrophys.*, 2006, **449**, 1297–1309.
- 75 F. Long, P. Pinilla, G. J. Herczeg, D. Harsono, G. Dipierro, I. Pascucci, N. Hendler, M. Tazzari, E. Ragusa, C. Salyk, S. Edwards, G. Lodato, G. van de Plas, D. Johnstone, Y. Liu, Y. Boehler, S. Cabrit, C. F. Manara, F. Menard, G. D. Mulders, B. Nisini, W. J. Fischer, E. Rigliaco, A. Banzatti, H. Avenhaus and M. Gully-Santiago, *Astrophys. J.*, 2018, **869**, 17.
- 76 H. J. Fraser, M. P. Collings, M. R. S. McCoustra and D. A. Williams, *Mon. Not. R. Astron. Soc.*, 2001, **327**, 1165–1172.
- 77 G. D. Mulders, I. Pascucci and D. Apai, *Astrophys. J.*, 2015, **798**, 112.
- 78 M. Minissale, Y. Aikawa, E. Bergin, M. Bertin, W. A. Brown, S. Cazaux, S. B. Charnley, A. Coutens, H. M. Cuppen, V. Guzman, H. Linnartz, M. R. S. McCoustra, A. Rimola, J. G. M. Schrauwen, C. Toubin, P. Ugliengo, N. Watanabe, V. Wakelam and F. Dulieu, *ACS Earth and Space Chemistry*, 2022, **6**, 597–630.
- 79 J. Li, E. A. Bergin, G. A. Blake, F. J. Ciesla and M. M. Hirschmann, *Science Advances*, 2021, **7**, eabd3632.
- 80 M. Asplund, A. M. Amarsi and N. Grevesse, *Astron. Astrophys.*, 2021, **653**, A141.
- 81 R. Meijerink, K. M. Pontoppidan, G. A. Blake, D. R. Poelman and C. P. Dullemond, *Astrophys. J.*, 2009, **704**, 1471–1481.
- 82 A. J. Greenwood, I. Kamp, L. B. F. M. Waters, P. Woitke and W. F. Thi, *Astron. Astrophys.*, 2019, **626**, A6.
- 83 R. Kuiper, H. Klahr, H. Beuther and T. Henning, *Astrophys. J.*, 2011, **732**, 20.
- 84 B. Zhao, K. Tomida, P. Hennebelle, J. J. Tobin, A. Maury, T. Hirota, Á. Sánchez-Monge, R. Kuiper, A. Rosen, A. Bhandare, M. Padovani and Y.-N. Lee, *Space Sci. Rev.*, 2020, **216**, 43.
- 85 P. D'Alessio, J. Cantó, N. Calvet and S. Lizano, *Astrophys. J.*, 1998, **500**, 411–427.
- 86 P. Nazari, B. Tabone, G. P. Rosotti, M. L. van Gelder, R. Meshaka and E. F. van Dishoeck, *Astron. Astrophys.*, 2022, **663**, A58.
- 87 P. Nazari, B. Tabone and G. P. Rosotti, *arXiv e-prints*, 2022,

- arXiv:2211.00126.
- 88 C. P. Dullemond, A. Juhasz, A. Pohl, F. Sereshti, R. Shetty, T. Peters, B. Commercon and M. Flock, *RADMC-3D: A multi-purpose radiative transfer tool*, Astrophysics Source Code Library, record ascl:1202.015, 2012.
  - 89 A. D. Bosman, E. A. Bergin, J. K. Calahan and S. E. Duval, *Astrophys. J. Lett.*, 2022, **933**, L40.
  - 90 E. F. van Dishoeck, E. Herbst and D. A. Neufeld, *Chemical Reviews*, 2013, **113**, 9043–9085.
  - 91 D. Baulch, C. Cobos, R. Cox, C. Esser, P. Frank, T. Just, J. Kerr, M. Pilling, J. Troe, R. Walker and J. Warnatz, *J. Phys. Chem. Ref. Data*, 1992, **21**, 411–734.
  - 92 T. Bethell and E. Bergin, *Science*, 2009, **326**, 1675.
  - 93 R. Visser, E. F. van Dishoeck, S. D. Doty and C. P. Dullemond, *Astron. Astrophys.*, 2009, **495**, 881–897.
  - 94 D. Bockelée-Morvan, D. C. Lis, J. E. Wink, D. Despois, J. Crovisier, R. Bachiller, D. J. Benford, N. Biver, P. Colom, J. K. Davies, E. Gérard, B. Germain, M. Houde, D. Mehringer, R. Moreno, G. Paubert, T. G. Phillips and H. Rauer, *Astron. Astrophys.*, 2000, **353**, 1101–1114.
  - 95 M. N. Drozdovskaya, E. F. van Dishoeck, M. Rubin, J. K. Jørgensen and K. Altwegg, *Mon. Not. R. Astron. Soc.*, 2019, **490**, 50–79.
  - 96 M. P. Collings, M. A. Anderson, R. Chen, J. W. Dever, S. Viti, D. A. Williams and M. R. S. McCoustra, *Mon. Not. R. Astron. Soc.*, 2004, **354**, 1133–1140.
  - 97 M. Vlasblom, and et al., *A&A in prep.*, 2023.
  - 98 A. D. Bosman, E. A. Bergin, J. Calahan and S. E. Duval, *Astrophys. J. Lett.*, 2022, **930**, L26.
  - 99 A. E. Glassgold and J. R. Najita, *Astrophys. J.*, 2015, **810**, 125.
  - 100 M. Ádámkóvics, A. E. Glassgold and J. R. Najita, *Astrophys. J.*, 2014, **786**, 135.
  - 101 S. Antonellini, I. Kamp, P. Riviere-Marichalar, R. Meijerink, P. Woitke, W. F. Thi, M. Spaans, G. Aresu and E. Lee, *Astron. Astrophys.*, 2015, **582**, A105.
  - 102 S. Antonellini, I. Kamp, F. Lahuis, P. Woitke, W. F. Thi, R. Meijerink, G. Aresu, M. Spaans, M. Güdel and A. Liebhart, *Astron. Astrophys.*, 2016, **585**, A61.
  - 103 M. Temmink, and et al., *A&A in prep.*, 2023.
  - 104 C. Salyk, G. A. Blake, A. C. A. Boogert and J. M. Brown, *Astrophys. J.*, 2009, **699**, 330–347.
  - 105 K. M. Pontoppidan, G. A. Blake, E. F. van Dishoeck, A. Smette, M. J. Ireland and J. Brown, *Astrophys. J.*, 2008, **684**, 1323–1329.
  - 106 S. Antonellini, A. Banzatti, I. Kamp, W. F. Thi and P. Woitke, *Astron. Astrophys.*, 2020, **637**, A29.
  - 107 GRAVITY Collaboration, K. Perraut, L. Labadie, J. Bouvier, F. Ménard, L. Klarmann, C. Dougados, M. Benisty, J. P. Berger, Y. I. Bouarour, W. Brandner, A. Caratti O Garatti, P. Caselli, P. T. de Zeeuw, R. Garcia-Lopez, T. Henning, J. Sanchez-Bermudez, A. Sousa, E. van Dishoeck, E. Alécian, A. Amorim, Y. Clénet, R. Davies, A. Drescher, G. Duvert, A. Eckart, F. Eisenhauer, N. M. Förster-Schreiber, P. Garcia, E. Gendron, R. Genzel, S. Gillessen, R. Grellmann, G. Heißel, S. Hippler, M. Horrobin, Z. Hubert, L. Jocou, P. Kervella, S. Lacour, V. Lapeyrière, J. B. Le Bouquin, P. Léna, D. Lutz, T. Ott, T. Paumard, G. Perrin, S. Scheithauer, J. Shangguan, T. Shimizu, J. Stadler, O. Straub, C. Straubmeier, E. Sturm, L. Tacconi, F. Vincent, S. von Fellenberg and F. Widmann, *Astron. Astrophys.*, 2021, **655**, A73.
  - 108 A. Miotello, E. F. van Dishoeck, J. P. Williams, M. Ansdell, G. Guidi, M. Hogerheijde, C. F. Manara, M. Tazzari, L. Testi, N. van der Marel and S. van Terwisga, *Astron. Astrophys.*, 2017, **599**, A113.
  - 109 L. I. Cleeves, R. A. Loomis, R. Teague, E. A. Bergin, D. J. Wilner, J. B. Bergner, G. A. Blake, J. K. Calahan, P. Cazzolletti, E. F. van Dishoeck, V. V. Guzmán, M. R. Hogerheijde, J. Huang, M. Kama, K. I. Öberg, C. Qi, J. Terwisscha van Scheltinga and C. Walsh, *Astrophys. J.*, 2021, **911**, 29.
  - 110 A. D. Bosman, F. Alarcón, E. A. Bergin, K. Zhang, M. L. R. van't Hoff, K. I. Öberg, V. V. Guzmán, C. Walsh, Y. Aikawa, S. M. Andrews, J. B. Bergner, A. S. Booth, G. Cataldi, L. I. Cleeves, I. Czekala, K. Furuya, J. Huang, J. D. Ilee, C. J. Law, R. Le Gal, Y. Liu, F. Long, R. A. Loomis, F. Ménard, H. Nomura, C. Qi, K. R. Schwarz, R. Teague, T. Tsukagoshi, Y. Yamato and D. J. Wilner, *Astrophys. J. Suppl. Ser.*, 2021, **257**, 7.
  - 111 A. Banzatti, I. Pascucci, A. D. Bosman, P. Pinilla, C. Salyk, G. J. Herczeg, K. M. Pontoppidan, I. Vazquez, A. Watkins, S. Krijt, N. Hendler and F. Long, *Astrophys. J.*, 2020, **903**, 124.
  - 112 A. D. Bosman and A. Banzatti, *Astron. Astrophys.*, 2019, **632**, L10.
  - 113 M. K. McClure, *Astron. Astrophys.*, 2019, **632**, A32.
  - 114 J. A. Sturm, M. K. McClure, D. Harsono, S. Facchini, F. Long, M. Kama, E. A. Bergin and E. F. van Dishoeck, *Astron. Astrophys.*, 2022, **660**, A126.
  - 115 S. M. Andrews, J. Huang, L. M. Pérez, A. Isella, C. P. Dullemond, N. T. Kurtovic, V. V. Guzmán, J. M. Carpenter, D. J. Wilner, S. Zhang, Z. Zhu, T. Birnstiel, X.-N. Bai, M. Benisty, A. M. Hughes, K. I. Öberg and L. Ricci, *Astrophys. J. Lett.*, 2018, **869**, L41.
  - 116 R. A. Booth and J. D. Ilee, *Mon. Not. R. Astron. Soc.*, 2019, **487**, 3998–4011.
  - 117 A. D. Bosman, A. G. G. M. Tielens and E. F. van Dishoeck, *Astron. Astrophys.*, 2018, **611**, A80.
  - 118 A. S. Booth, C. Walsh, J. D. Ilee, S. Notsu, C. Qi, H. Nomura and E. Akiyama, *Astrophys. J. Lett.*, 2019, **882**, L31.
  - 119 K. Zhang, E. A. Bergin, K. Schwarz, S. Krijt and F. Ciesla, *Astrophys. J.*, 2019, **883**, 98.
  - 120 S. Krijt, A. D. Bosman, K. Zhang, K. R. Schwarz, F. J. Ciesla and E. A. Bergin, *Astrophys. J.*, 2020, **899**, 134.
  - 121 M. E. Kress, A. G. G. M. Tielens and M. Frenklach, *Advances in Space Research*, 2010, **46**, 44–49.
  - 122 D. E. Anderson, E. A. Bergin, G. A. Blake, F. J. Ciesla, R. Visser and J.-E. Lee, *Astrophys. J.*, 2017, **845**, 13.
  - 123 H.-P. Gail and M. Tieloff, *Astron. Astrophys.*, 2017, **606**, A16.



- 124 C. F. Chyba, P. J. Thomas, L. Brookshaw and C. Sagan, *Science*, 1990, **249**, 366–373.
- 125 Y. Kebukawa, S. Nakashima and M. E. Zolensky, *Meteoritics and Planetary Science Suppl.*, 2010, **45**, 99–113.
- 126 M. Frenklach and E. D. Feigelson, *Astrophys. J.*, 1989, **341**, 372.
- 127 J. Morgan, W. A., E. D. Feigelson, H. Wang and M. Frenklach, *Meteoritics*, 1991, **26**, 374.
- 128 P. M. Woods and K. Willacy, *Astrophys. J. Lett.*, 2007, **655**, L49–L52.
- 129 A. Arabhavi, and et al., *subm.*, 2023.
- 130 I. Pascucci, D. Apai, K. Luhman, T. Henning, J. Bouwman, M. R. Meyer, F. Lahuis and A. Natta, *Astrophys. J.*, 2009, **696**, 143–159.
- 131 D. Semenov and D. Wiebe, *Astrophys. J. Suppl. Ser.*, 2011, **196**, 25.
- 132 P. Woitke, A. M. Arabhavi, I. Kamp and W. F. Thi, *Astron. Astrophys.*, 2022, **668**, A164.
- 133 S. M. Blevins, K. M. Pontoppidan, A. Banzatti, K. Zhang, J. R. Najita, J. S. Carr, C. Salyk and G. A. Blake, *Astrophys. J.*, 2016, **818**, 22.
- 134 A. D. Bosman and E. A. Bergin, *Astrophys. J. Lett.*, 2021, **918**, L10.
- 135 A. Morbidelli, J. Szulágyi, A. Crida, E. Lega, B. Bitsch, T. Tanigawa and K. Kanagawa, *Icarus*, 2014, **232**, 266–270.
- 136 R. Teague, J. Bae and E. A. Bergin, *Nature*, 2019, **574**, 378–381.
- 137 J.-E. Lee, E. A. Bergin and H. Nomura, *Astrophys. J. Lett.*, 2010, **710**, L21–L25.
- 138 A. M. Mandell, J. Bast, E. F. van Dishoeck, G. A. Blake, C. Salyk, M. J. Mumma and G. Villanueva, *Astrophys. J.*, 2012, **747**, 92.
- 139 A. D. Bosman, S. Bruderer and E. F. van Dishoeck, *Astron. Astrophys.*, 2017, **601**, A36.
- 140 P. Woitke, I. Kamp, S. Antonellini, F. Anthonioz, C. Baldwin-Saveedra, A. Carmona, O. Dionatos, C. Dominik, J. Greaves, M. Güdel, J. D. Ilee, A. Liebhart, F. Menard, M. Min, C. Pinte, C. Rab, L. Rigon, W. F. Thi, N. Thureau and L. B. F. M. Waters, *Publ. Astron. Soc. Pac.*, 2019, **131**, 064301.